International Journal of Physical Sciences

Academic Journals

ABOUT IJPS

The **International Journal of Physical Sciences (IJPS)** is published weekly (one volume per year) by Academic Journals.

International Journal of Physical Sciences (IJPS) is an open access journal that publishes high-quality solicited and unsolicited articles, in English, in all Physics and chemistry including artificial intelligence, neural processing, nuclear and particle physics, geophysics, physics in medicine and biology, plasma physics, semiconductor science and technology, wireless and optical communications, materials science, energy and fuels, environmental science and technology, combinatorial chemistry, natural products, molecular therapeutics, geochemistry, cement and concrete research, metallurgy, crystallography and computer-aided materials design. All articles published in IJPS are peer-reviewed.

Contact Us

International Journal of Physical Sciences

ARTICLES

Full Length Research Paper

Optical properties of ZnO thin films deposed by RF magnetron

R. Ondo-Ndong[1,2]*, H. Z. Moussambi[1], H. Gnanga[1], A. Giani[2] and A. Foucaran[2]

[1]Laboratoire pluridisciplinaire des sciences, Ecole Normale Supérieure, B.P 17009 Libreville, Gabon.
[2]Institut Electronique du Sud, IES-Unité mixte de Recherche du CNRS n° 5214, Université Montpellier II, Place E. Bataillon, 34095 Montpellier cedex 05- France.

We have grown ZnO thin films on glass substrate by RF magnetron sputtering using metallic zinc target. The influences of some parameters on thin film optical properties were assessed. They exhibited extremely high resistivity of 10^{12} Ω.cm, an energy gap of 3.3 eV at room temperature. It was found that a RF power of 50 W, a target to substrate distance of 70 mm, very low gas pressures of 3.35 x 10^{-3} Torr of argon and oxygen mixed gas atmosphere gave ZnO thin films with a good homogeneity and a high crystallinity. All the films are transparent in the visible region (400 to 800 nm) with average transmittance above 80%. The optical transmittance and refractive index, calculated from the spectra of optical absorbance, show a significant dependence on the growth parameters. As for the sample grown at 100°C, the average transmittance is about 80% in the visible wavelength range and the refractive index is estimated to be 1.97.

Key words: ZnO, RF sputtering magnetron, X-ray diffraction, transmittance, refractive index.

INTRODUCTION

Zinc oxide is one of the most interesting II–IV compound semiconductors with a wide direct band gap of 3.3 eV (Meng and Dos Santos, 1994; Inukai et al., 1995; Han and Jou, 1995; Craciun et al., 1995; Subramanyam et al., 1999; Sanchez-Juarez et al., 1998; Sourdi et al., 2012; Yang Ming Lu et al., 2007). It has been investigated extensively because of its interesting electrical, optical and piezoelectric properties making suitable for many applications such as transparent conductive films, solar cell window and MEMS waves devices (Craciun et al., 1995). The thermal stresses were determined by using a bending-beam Thorton method (Han and Jou, 1995) while thermally cycling films. ZnO has hexagonal Wurtzite structure and some properties are determined by the crystallite orientation on the substrate. For example, for piezoelectric applications, the crystallite should have the c-axis perpendicular to the substrate. According to the literature, the reactive sputtering technique has received a great interest because of its advantages for film growth, such as easy control for the preferred crystalline orientation, epitaxial growth at relatively low temperature, good interfacial adhesion to the substrate and the high packing density of the grown film. These properties are mainly caused by the kinetic energy of the clusters given

by electric field (Molarius et al., 2003; Lin et al., 2008; Kim et al., 1997). This energy enhances the surface migration effect and surface bonding state.

In previous work, we investigated the effect of the substrate temperature and the oxygen-argon mixture gas on the properties of ZnO films. It has been found that the structural properties of ZnO films depend very much on the substrate temperature. Indeed, a ZnO hexagonal wurtzite structure and properties are determined by the orientation of the crystallites on the substrate. FWHM of the (002) X-ray rocking curve must be less than 0.32 for an effective electromechanical coupling (Ondo-Ndong et al., 2003). In continuation of this work, the optical properties of ZnO structures have been investigated based on the deposition parameters.

EXPERIMENTAL

Zinc oxide films were deposited by RF magnetron sputtering using a zinc target (99, 99%) with diameter of 51 and 6 mm thick. Substrate is p-type silicon with (100) orientation. The substrates were thoroughly cleaned with organic. Magnetron sputtering was carried out in an oxygen and argon mixed gas atmosphere by supplying RF power at a frequency of 13.56 MHz. The RF power was about 50 W. The flow rates of both the argon and oxygen were controlled by using flow meter (ASM, AF 2600). The sputtering pressure was maintained at $3.35.10^{-3}$ torr controlling by a Pirani gauge. Before deposition, the pressure of the sputtering system was under 4.10^{-6} torr for more than 12 h and were controlled by using an ion gauge controller (IGC – 16 F).

Thin films were deposited on silicon, substrate under conditions listed in Table 1. These deposition conditions were fixed in order to obtain the well-orientation zinc oxide films. The presputtering occurred for 30 min to clean the target surface. Deposition rates covered the range from 0.35 to 0.53 μm/h. All films were annealed in helium ambient at 650°C for 15 mn. Measurements of transmittance in the range from 300 to 900 nm are made using a UV-Visible CARY spectrometer.

The device has a pulsed xenon lamp, which produces only a flash in each acquisition of a measurement point. A quartz bulb, not glass, let's UV radiation through. The emerging beam is then a cylindrical diverging beam that will cover the entire surface of the mirror M1. A mirror allows the orientation and focus of the useful part of the beam emerging from the input to the network and then diffracted by the latter towards a beam exit slot gap. The assembly constituted by the entrance slit and the first mirror is called collimator. A blade placed on the path L of monochromatic radiation is used to reflect a portion of the intensity of the wave to a photoreceptor which measures the intensity of radiation which will pass through the vessel containing the sample to take into account small fluctuations the intensity of the light source. The rough surface materials with in homogeneities or imply low volume detected signal. Thus, we must make an adjustment, before any measurement: The 100% for power transmission Pyrex substrate as a reference. Piloting, digital capture and processing of data is performed by a microcomputer.

Theoretical model for complex index

To calculate the optical constants, are often used to model on a volume of isotropic and homogeneous material. In reality, the behavior of thin films obtained from the ideal model overflows due to the inhomogeneity of layers and the dispersion of the refractive.

Table 1. ZnO sputtering conditions.

Sputtering pressure	3.35×10^{-3} Torr
Mixture gas	$A_r + O_2$ = 80 – 20%
Power RF	50 W
Sputtering time	6 h
Substrate temperature	100°C
Target-substrate distance	7 cm

These optical constants are represented by the index of refraction that is, in the general case, depends on the complex wavelength dependence $\tilde{n} = n(\lambda) + ik(\lambda)$. Is the real part of the refractive index. The complex index $\tilde{n} = n(\lambda) + ik(\lambda)$ is very important for the dielectric characterization of materials. $\tilde{n}$ Provides, at infinity, the complex permittivity $\tilde{\varepsilon} = \varepsilon_1 + i\varepsilon_2$ through:

$$\varepsilon_1 = n^2 - k^2$$
$$\varepsilon_2 = 2n \cdot k$$

And also, the relative permittivity ε_r and electrical conductivity to the required frequency σ through:

$$\varepsilon_r = \varepsilon_1$$
$$\sigma = \varepsilon_2 \cdot \omega \cdot \varepsilon_0$$

The measurement of light transmission through a parallel plate dielectric film, in the working range considered, is sufficient to determine the real and imaginary parts of the complex refractive index and thickness. Wales and Lyashenko developed a method using the successive approximations and interpolations for calculating these three quantities (Wales et al., 1967; Lyashenko and Miloslavskii, 1964).

Manifacier et al. (1976) have developed a method, like in the same range of applicability but differs from Lyashenko and Miloslavskii (1964) accuracy by: Firstly, the calculation processing and the data is easier, and secondly it provides an explicit expression for n, k and thickness. This last method we have used to characterize our samples of zinc oxide thin film prepared. Figure 1 shows a thin layer complex refractive index $\tilde{n}$, linked by two transparent media n_1 and index n_0. With n_0 the index of air ($n_0 = 1$) and n_1 the index of the substrate.

In the case of normal incidence, the amplitude of the transmitted wave length is given by Wales et al. (1967) and Lyashenko and Miloslavskii (1964):

$$A = \frac{t_1 t_2 \exp(-2i\pi nd/\lambda)}{1 + r_1 r_2 \exp(-4i\pi nd/\lambda)} \tag{1}$$

Where t_1, t_2, r_1, r_2, n and d are respectively the transmission and reflection coefficients of the front and rear faces of the sample, the refractive index and the thickness of the material. The transmission of the layer is given by:

$$T = n_1/n_0 \mid A \mid^2 \tag{2}$$

In the case of low absorption along with,

$$k^2 \ll (n - n_0)^2 \text{ et } k^2 \ll (n - n_1)^2 \tag{3}$$
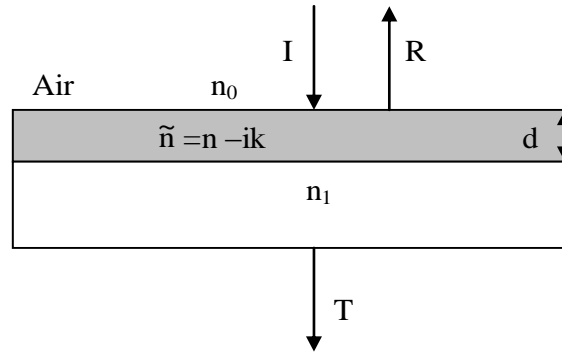
Figure 1. Optical transmittance on the sample.
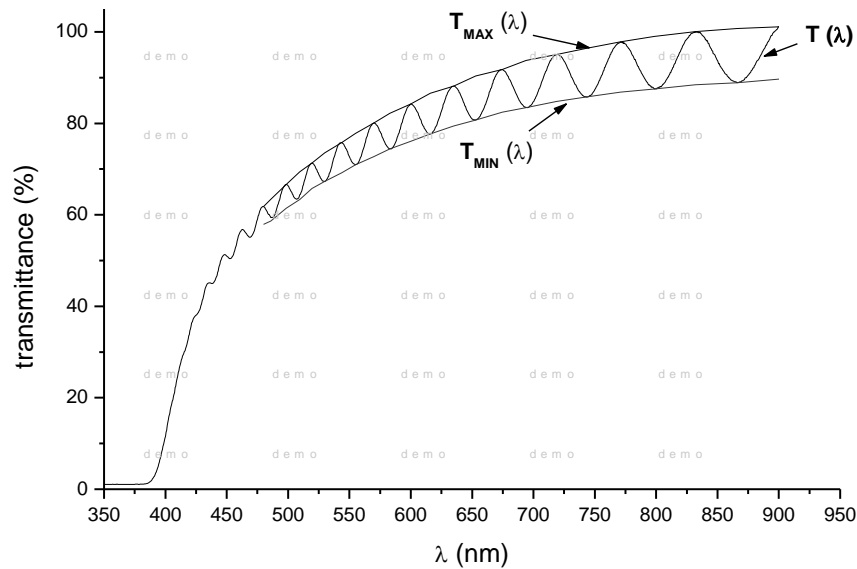
Figure 2. Optical transmittance spectra Example on the sample.

$$T = \frac{16 n_0 n_1 n^2 \alpha}{C_1^2 + C_2^2 + 2 C_1 C_2 \alpha \cos 4n\,\pi d/\lambda} \tag{4}$$

Where $C_1 = (n + n_0)(n_1 + n)$, $C_2 = (n - n_0)(n_1 - n)$ (5)

And $\alpha = \exp(-4\pi kd/\lambda) = \exp(-\beta d)$ (6)

β is the absorption coefficient of the thin film, k is the extinction coefficient and the percentage absorption α.

Generally, outside the region of the fundamental absorption or free carrier absorption (for higher wave lengths), the dispersions of n and k are large. The maxima and minima of transmission in Equation (4) to occur:

$$\frac{4\pi nd}{\lambda} = m\pi \tag{7}$$

Where m is the wave number.

In corresponding to a thin layer of transparent semiconductor substrate non-absorbent, $C_2 < 0$ usual cases, the extreme values of the transmission are given by the formula:

$$T_{max} = \frac{16 n_0 n_1 n^2 \alpha}{(C_1 + \alpha C_2)^2}, \quad T_{min} = \frac{16 n_0 n_1 n^2 \alpha}{(C_1 - \alpha C_2)^2} \tag{8}$$

Combining Equations (8) relationship Lyashenko developed an iterative method for the determination of n and α, and using Equations (6) and (7), determining k and d. We propose a major simplification of this method. Indeed, we consider T_{min} and T_{max} as continuous functions of n (λ) and α (λ). Indeed, the two envelopes of the measured transmittance form a non-linear system of two equations in two unknowns n (λ) and α (λ), which can be solved by iteration. These functions, which are envelopes of the maxima T_{max} (λ) and the minimum T_{min} (λ) in the transmission spectrum are shown in Figure 2. α coefficient is given by the ratio of Equations (8).

$$\alpha = \frac{C_1 \left[1 - (T_{max} / T_{min})^{1/2} \right]}{C_2 \left[1 + (T_{max} / T_{min})^{1/2} \right]} \tag{9}$$
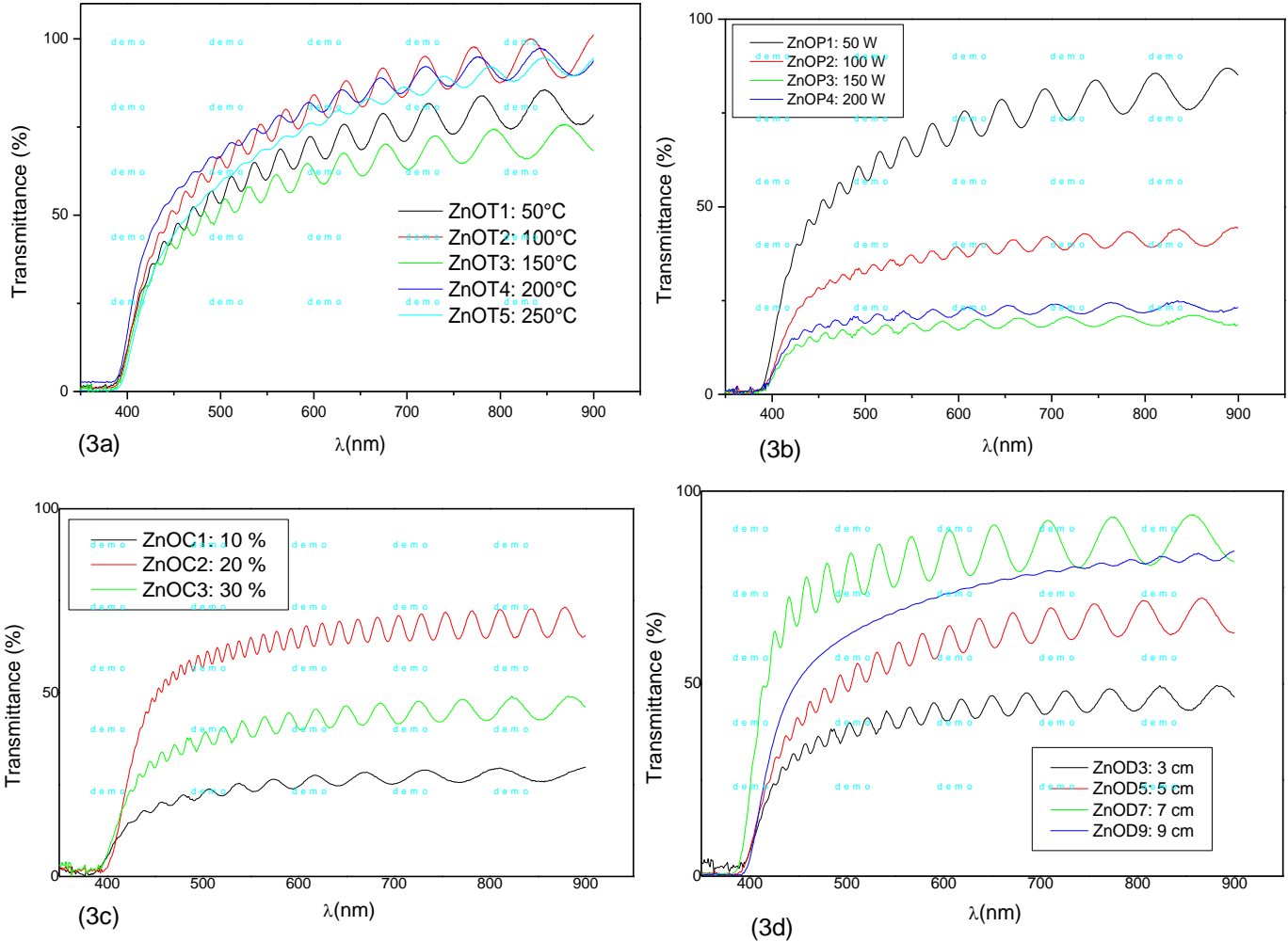
Figure 3. Optical transmittance spectra of ZnO thin films: a) at various substrate temperatures, b) at different power, c) based on the rate of oxygen, d) depending on the target-substrate distance.

Then we deduce Equation (8) the relationship of the refractive index of the thin layer.

$$n = \left[N + \left(N^2 - n_0^2 n_1^2 \right)^{1/2} \right]^{1/2} \quad (10)$$

With $\quad N = \dfrac{n_0^2 + n_1^2}{2} + 2n_0 n_1 \dfrac{T_{max} - T_{min}}{T_{max} T_{min}} \quad (11)$

N is a constant.

The Equation (8) shows that the refractive index n is determined explicitly.

Knowing n can be determined by the above equation α. The thickness d of the layer may be calculated by two maxima or minima using the equation below.

$$d = \frac{M \lambda_1 \lambda_2}{2 \left[n(\lambda_1) \lambda_2 - n(\lambda_2) \lambda_1 \right]} \quad (12)$$

Where in M is the number of oscillations between two extreme points (M =1 between two consecutive minima or M=2 two

consecutive maxima), λ_1, n (λ_1) and λ_2, n (λ_2) levels are matching wave the wavelength and the refractive index.

RESULTS AND DISCUSSION

Transmittance

To know the parameter values that seem to be making the best deposits from a structural point of view, we have undertaken, optical characterizations in order to identify the influence of the four parameters of deposits. And to avoid the effect of film thickness on the optical properties, we worked on samples of similar thicknesses of 2.8 to 2.9 μm.

Figure 3 shows the transmission spectra of ZnO films. We observe that the powers in Figure 3a transmission are high (80 to 90%) for all samples. It is also observed that the absorption front at a wavelength for which the transmission is reduced to 50% is set to 375 to 400 nm.
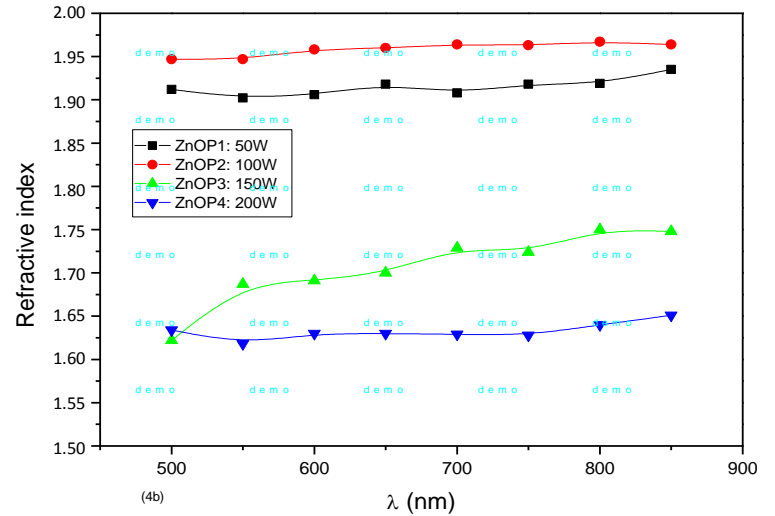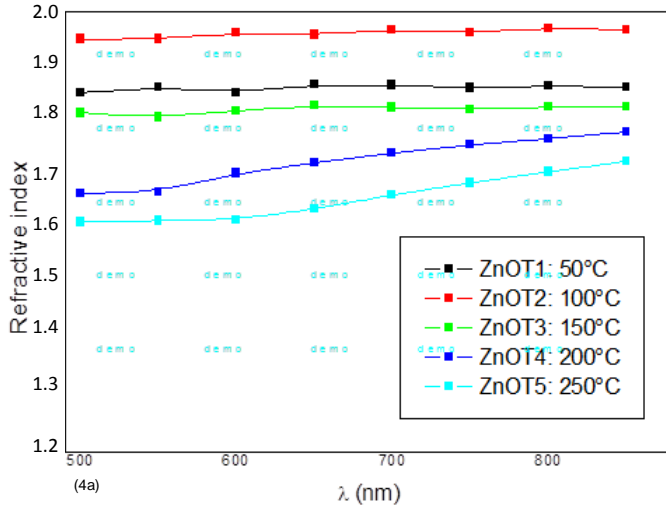
Figure 4. Refractive index as a function of wavelength: a) for different substrate temperatures; b) different powers.

The difference of the extreme of all samples was 100°C maximum in Figure 3a. Subramanyam et al. (1999) confirm these results. Indeed, they get a power transmission of the order 86% and observed a decrease in optical transmission with temperature in the range 300-400°C.

In the spectral range considered, we have represented in Figure 3b changing transmission thin zinc oxide layers for different powers. We note that the sample of ZnO prepared to 50 W has a maximum transmission of about 80%. By cons, for the other samples, the transmission spectra are of little use. These observations clearly confirm the results obtained by ray diffraction where we found that the samples are poorly crystallized and the grain size is unusually small compared to that obtained with the sample 50 W. The effect of oxygen on the transmission rate of the ZnO films showed in Figure 3c. A decrease in transmittance was observed to measure the percentage of oxygen in the gas mixture ($Ar - O_2$) increases in the region of short wavelength. The maximum transmission is observed for the oxygen content equal to 20% and the minimum transmission are higher. Moreover, the difference between the transmissions of the extrema ($T_{max} - T_{min}$) is greater for the sample. This reflects a higher refractive index.

We studied the influence of the target-substrate distance watching the optical transmission of the ZnO thin films. Figure 3d shows that the optical properties of zinc oxide are dependent of the target-substrate distance. Based on the experimental conditions, we can say that the target-substrate distance equal to 7 cm is ideal for making our ZnO films. Indeed, the power transmission of this sample was very high (95% λ = 600 nm). It is estimated to have homogeneous layer thickness minimum distance. Indeed, at this distance, the

thermalization of the structure is efficient. The discharge (plasma) is maintained with a minimum of particle collision and the efficiency of the pulverization is effective.

Refractive index n

Changes in the refractive index as a function of wavelength at different substrate temperatures are shown in Figure 4a. The refractive index has a high dispersion to the layers developed to above 150°C temperatures. Figure 4b shows the variation of the refractive index as a function of wavelength at different powers. We see that the index decreases with power. It varies from 1.97 to 1.6 in from 50 to 200W at 600 nm. Figure 5 shows that a given wavelength, the refractive index increases from 1.87 to 1.97 when the substrate temperature ranges from 50 to 100°C. Above 100°C, the value of the refractive index decreases as the substrate temperature increases to 1.63. To highlight these observations, we have shown in Figure 6 changes in the refractive index as a function of oxygen concentration in the gas mixture at a given wavelength (λ = 600 nm). We find that the influence of the gas mixture on the refractive index is significant only when we have an oxygen level of 20%. In addition, we note a decrease in the index with increasing oxygen content in the gas mixture. We attribute this phenomenon, compared with the X-ray crystallographic disorientation of the structure. Indeed, the structural study showed that the optimum oxygen level, to develop well-crystallized films of ZnO was 20%.

Figure 7 shows that the target distance of 7 cm substrate is ideal for obtaining zinc oxide layers of good quality, taking into account, of course, the deposition
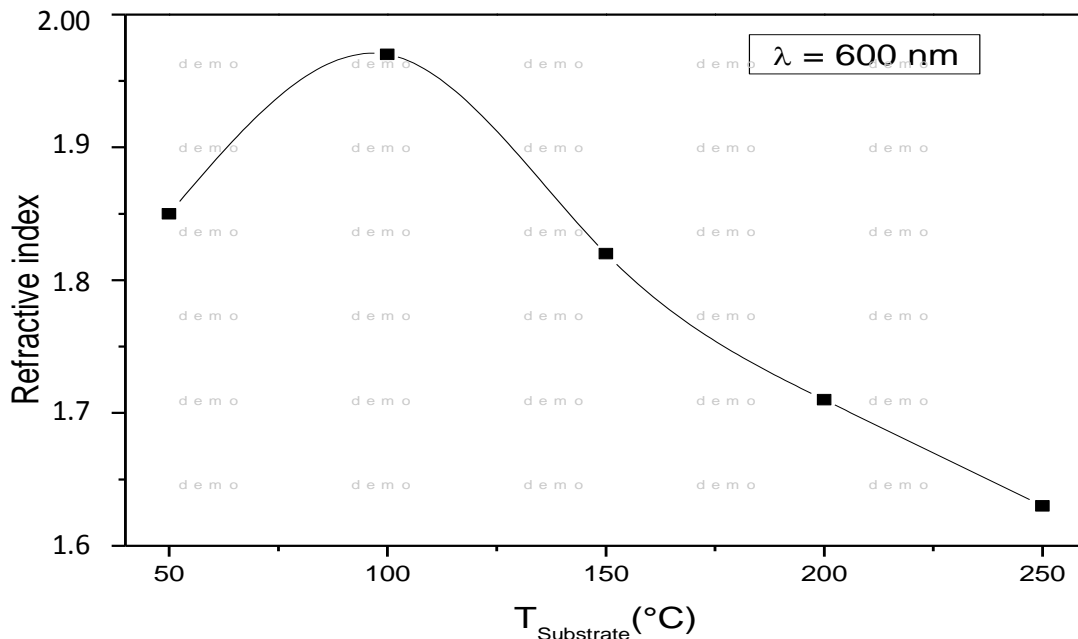
Figure 5. Refractive index as a function of the substrate temperature constant λ.
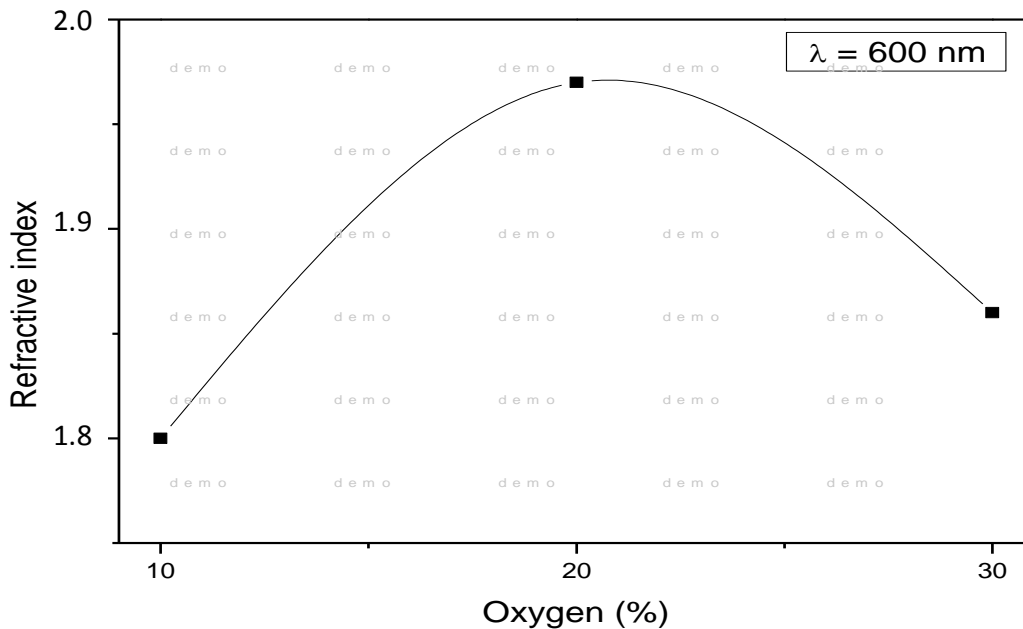
Figure 6. Refractive index as a function of oxygen concentration at constant λ.

conditions. Knowing that the optical properties of thin films depend on the thickness, we determined the thickness of our ZnO films by Equation (12) and we have compared to values determined by profilometry. Figure 8 shows the variation of the thickness of the ZnO thin film as a function of the launched power. We find that the thicknesses obtained by optical determination decrease as the power increases. This explains, perhaps, the low transmittance samples drawn over 50 W. In addition, the evolution of the diffraction peak as a function of RF power, shows that the samples prepared at most 50 W exhibit crystallization defects.
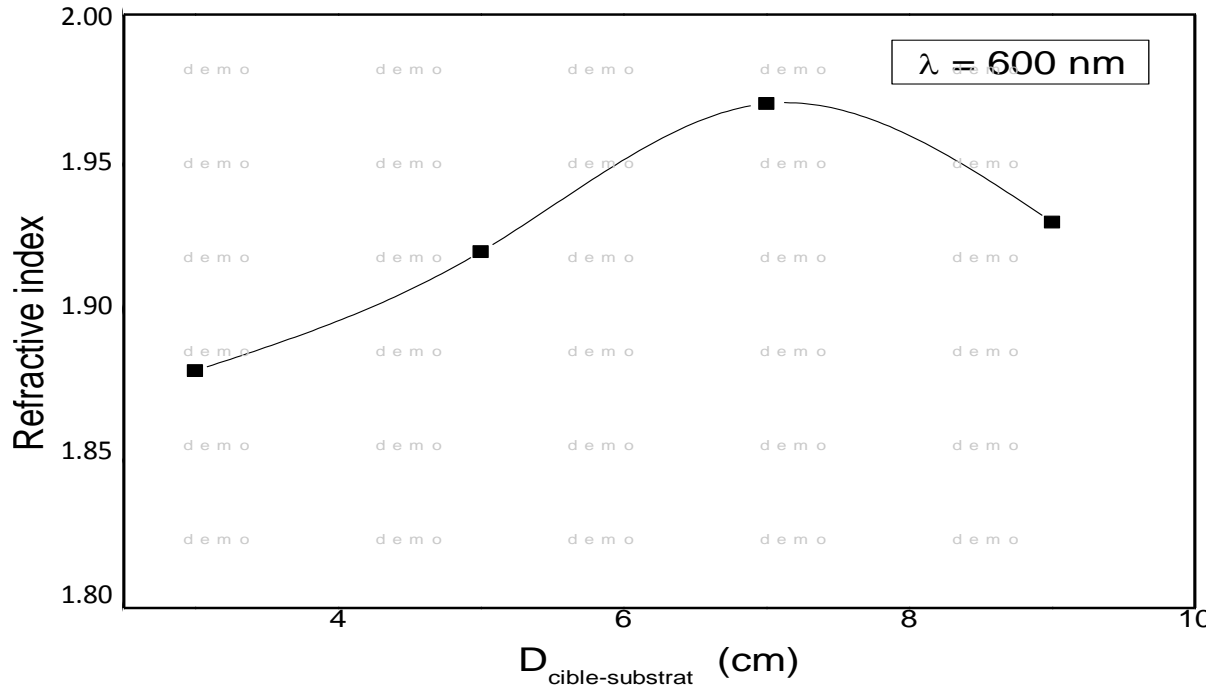
Figure 7. Refractive index as a function of the substrate-target distance constant λ.
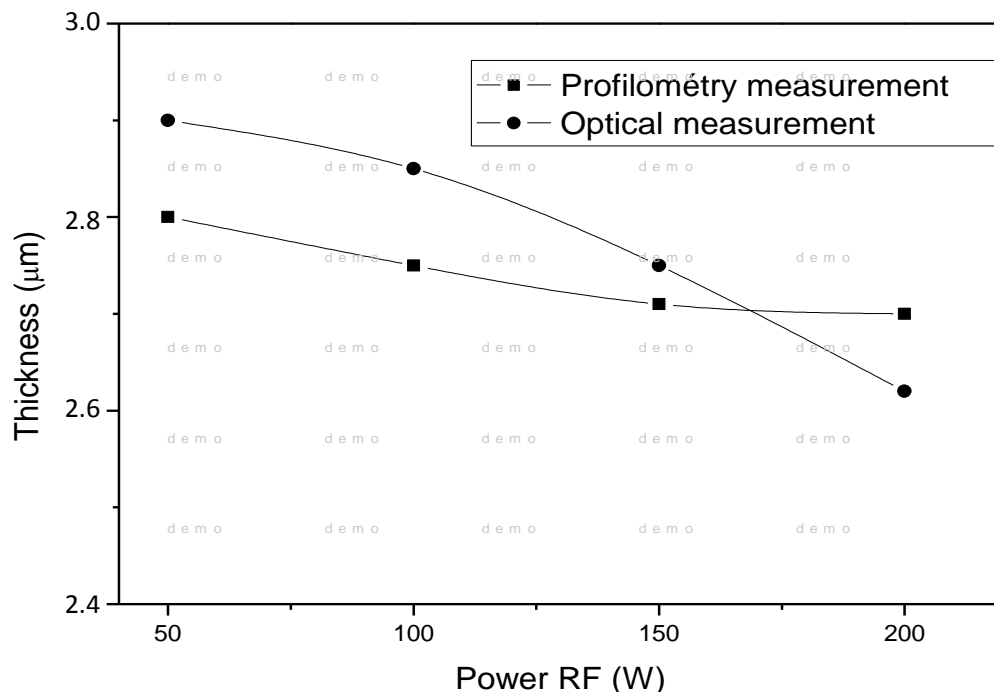
Figure 8. Evolution of the thickness of the ZnO film in function of the power RF.

Determination of the optical gap E_g

The X-ray part presents a spectrum of electromagnetic radiation. The wave-particle duality of radiation is expressed by such a relation between the energy of a photon, and the wavelength λ.
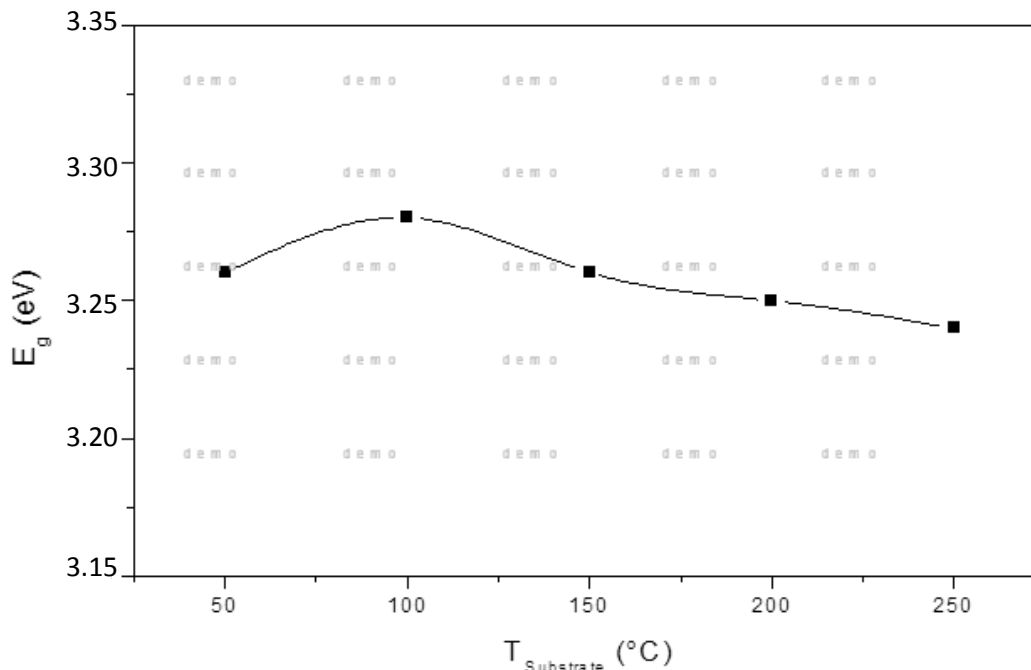
Figure 9. Dependence of the gap as a function of substrate temperature.

$$E = h\nu = \frac{hc}{\lambda} \quad \text{or} \quad \lambda = \frac{hc}{E} \tag{13}$$

The simple and well-known formula is:

$$\lambda_{nm} = \frac{1{,}24}{E(eV)} \tag{14}$$

It is from this relationship that we determine the energy of the band gap of our prepared by RF magnetron sputtering thin layers. In fact, we make a linear extrapolation at the absorption front of our power transmission layer. This straight line intersects the wavelength axis at a value of λ. For the different samples, we determined the optical gap from Equation (14). Indeed, the level of the linear variation of the absorption front, we drew a curve tangential to the front. This linear extrapolation, which cuts the axis of wavelengths, we can determine the optical gap. Figure 9 shows the evolution of the gap energy as a function of substrate temperature band. We find that the evolution of the energy of the forbidden band as a function of substrate temperature is almost constant. However, the sample prepared at 100°C gives an energy gap greater range compared to those given by the other samples.

Conclusion

Here, the effect on different experimental parameters on the growth and the properties of thin layers of zinc oxide has been studied. We performed several sets of samples we characterized optically. This systematic study led us to an area of very specific definition of manufacturing parameters for obtaining ZnO films of good quality. Indeed, the numerical parameters of the manufacturing balance sheet are as follows: 100°C for the substrate temperature, 50 W RF power injected into the discharge, 20% to the oxygen content in the gas mixture and 7 cm for the target-substrate distance.

These results, which are consistent with those found in the literature on zinc oxide prepared by RF magnetron sputtering, using a zinc target, will allow us to achieve the intended applications.

Conflict of Interest

The authors have not declared any conflict of interest.

REFERENCES

Craciun V, Elders J, Gardeniers JGE, Geretovsky J, Boyd IW (1995). Growth of ZnO thin films on GaAs by pulsed laser deposition. Thin Solid Films 259:1-4. doi:10.1016/0040-6090(94)09479-9

Han MY, Jou JH (1995). Determination of the mechanical properties of rf magnetron sputtered zinc oxide thin films on substrate. Thin Solid Films. 260:58-64. doi:10.1016/0040-6090(94)06459-8

Inukai T, Matsuoka M, Ono K (1995). Characteristics of zinc oxide thin films prepared by r.f. magnetron-mode electron cyclotron resonance sputtering. Thin Solid Films. 257:22-27. doi:10.1016/0040-6090(94)06325-7

Kim YJ, Kim YT, Yang HK, Park JC, Han JI, Lee YE, Kim HJ (1997). Epitaxial growth of zno thin films on r-plane sapphire substrate by radio frequency magnetron sputtering. J. Vacuum Sci. Technol. A. 15:1103-1107. DOI: 10.1116/1.580437

Lin YC, Hong CR, Chuang HA (2008). Fabrication and analysis of ZnO thin film bulk acoustic resonators. Appl. Surf. Sci. 254(13):3780-3786. doi:10.1016/j.apsusc.2007.11.059

Lyashenko SP, Miloslavskii VK (1964). A simple method for the determination of the thickness and optical constants of semiconducting and dielectric layers. Opt. Spectrosc. 16:80-81.

Manifacier JC, Gasiot J, Fillard JP (1976). A simple method for the determination of the optical constants n, k and the thickness of a weakly absorbing thin film. Phys. E: Sci. Instrum. 9(1976):1002. doi:10.1088/0022-3735/9/11/032

Meng LJ, Dos Santos MP (1994). Direct current reactive magnetron sputtered zinc oxide thin films the effect of the sputtering pressure. Thin Solid Films 250:26-32. doi:10.1016/0040-6090(94)90159-7

Molarius J, Kaitila J, Pensala T, Ylilammi M (2003). Piezoelectric ZnO films by r.f. sputtering. J. Mater. Sci.: J. Mater. Electron. 14:431-435. DOI: 10.1023/A:1023929524641

Ondo-Ndong R, Ferblantier G, Al Kalfioui M, Boyer A, Foucaran A (2003). Properties of rf magnetron sputtered zinc oxide thin films. J. Cryst. Growth. 255:130-135. doi:10.1016/S0022-0248(03)01243-0

Sanchez-Juarez A, Tiburcio-Silver A, Ortiz A, Zironi EP, Rickards J (1998). Electrical and optical properties of fluorine-doped ZnO thin films prepared by spray pyrolysis. Thin Solid Films 333:196-202. doi:10.1016/S0040-6090(98)00851-7

Sourdi I, Mamat MH, Abdullah MH, Ishak A, Rusop M (2012). Optical properties of nano-structured zinc oxide thin films deposited by radio-frequency magnetron sputtering at different substrate temperatures. Humanities, Science and Engineering Research (SHUSER), 2012 IEEE Symposium on 24-27 June 2012:607–611. DOI: 10.1109/SHUSER.2012.6268895

Subramanyam TK, Srinivasulu Naidu B, Uthanna S (1999). Structure and optical properties of dc reactive magnetron sputtered zinc oxide films. Cryst. Res. Technol. 34:981–988. DOI: 10.1002/(SICI)1521-4079(199909)34:8<981::AID-CRAT981>3.0.CO;2-G

Wales J, Lovitt GJ, Hill RA (1967). Optical properties of germanium films in the 1–5 μ range. Thin Solid Films. 1:137-150. doi:10.1016/0040-6090(67)90010-7.

Yang Ming L, Shu Yi T, Jeng Jong L, Min Hsiung H (2007). The structural and optical properties of zinc oxide thin films deposited on PET Substrate by r.f. Magnetron Sputtering. Solid State Phenomena.121–123 :971-974. 10.4028/www.scientific.net/SSP.121-123.971.

Full Length Research Paper

Behavior architecture controller for an autonomous robot navigation in an unknown environment to perform a given task

Jasmine Xavier A.[1]* and Shantha Selvakumari R.[2]

[1]Jayaraj Annapackiam CSI College of Engineering, Anna University, Chennai, Tamil Nadu India.
[2]Mepco Schlenk Engineering College, Anna University, Chennai, Tamil Nadu India.

The aim of this paper is to carry out navigation task in an unknown environment with high density obstacles using an autonomous mobile robot. Fuzzy logic approach is used for the robot planning because the output varies smoothly as the input changes. If the navigation environment contains one or more obstacles the robot must be able to avoid collisions. The robot uses the obstacle avoidance controller in order to reach the final destination safely without collision with these objects. The robot moves toward the goal and when an obstacle is detected in one of the three sides (front, left, right) the obstacle avoidance behavior is activated to generate the appropriate actions for avoiding these collisions.

Key words: Robot navigation, robot exploration, goal seeking.

INTRODUCTION

There is growing interest in applications of mobile robots. This is due to the fact that the robots are finding their way out of sealed working stations in factories to our homes and to populated places such as museum halls, office buildings, railway stations, department stores and hospitals (Shuzhi and Lewis, 2006). Mobile robots have been the object of many researchers over the last few years in order to improve their operational capabilities of navigation in an unknown environment which consist of the ability of the mobile robot to plan and execute a collision-free motion within its environment. However, this environment may be imprecise, complex and either partially or non-structured (Janglova, 2004). The path

planning problem of a mobile robot can be stated as: given the starting position of the robot, the target location and a description of its surrounding environment, plan a collision-free path between the specified points under satisfying an optimization criterion (Sugihara and Smith, 1997). The path planning in an unknown environment depends on the different sensory systems (cameras, sonar, etc.) which provide a global description of the surrounding environment of the mobile robot; therefore, this description might be associated with imprecision and uncertainty. Thus, to have a suitable path planning scheme, the controller must be robust to the imprecision of sensory measurements. Hence, the need for an

approach such as fuzzy logic (Ehsan et al., 2011; Beom and Cho, 1995) which can deal with uncertainties is more suitable for this kind of situations. In real-world problem for autonomous mobile robot navigation, it should be capable of sensing its environment, understanding the sensed information to receive the knowledge of its location and surrounding environment, planning a real-time path from a starting position to goal position with hurdle avoidance, and controlling the robot steering angle and its speed to reach the target. Fuzzy Logic is used in the design of possible solutions to perform local navigation, global navigation, path planning, steering control and speed control of a mobile robot. Fuzzy Logic (FL) and Artificial Neural Network (ANN) are used to assist autonomous mobile robot move, learn the environment and reach the desired target (Velappa et al., 2009). Fuzzy logic was used in many works to design robust controllers for the navigation of mobile robots in a cluttered environments and it can solve such complex real world problems within a reasonable accuracy and a low computational complexity, due to their heuristic nature. In addition, genetic algorithms (Seng et al., 1999), neural networks (Kian et al., 2002) and their combinations were developed to construct the fuzzy logic controller automatically. However, the fusion of different behaviors remains to be difficult when they attempt to control the same actuator simultaneously. Many efforts have been devoted to solve the problem of fusion behavior methods. Because of the complexity of the surrounding environment to be characterized or modeled accurately, behavior architecture control applications become important for the mobile robots navigation. It decomposes the navigation system into specific behavior. Behavior architecture modules which are connected directly to sensors and actuators and operate in parallel. Simple behaviors are then combined in order to produce a complex strategy able to pursue the strategic goals while effectively reacting to any contingencies. Therefore, this architecture can act in real-time and has good robustness. Brooks (1986) proposed an architecture that has been applied successfully in mobile robot navigation, but its main drawback is the arbitration technique which allows only the activation of one behavior at one time. In many situations, the activation of two behaviors is required, for example, when the robot is moving toward the target and avoids obstacles at the same time, two behaviors should be combined to fulfill this task (Yung and Ye, 1999). The basic idea in behavior based navigation is to subdivide the navigation task into small easy to manage, program and debug behaviors (simpler well defined actions) that focus on execution of specific subtasks. For example, basic behaviors could be "avoiding obstacles", "goal seeking" or "wall following". This divide and conquer approach has turned out to be a successful approach, for it makes the system modular, which both simplifies the navigation solution as well as offers a possibility to add new behaviors to the system

without causing any major increase in complexity (Brooks, 1989; Saffiotti, 1997). The suggested outputs from each concurrently active behavior are then "blended" together according to some action coordination rule (Fatmi et al., 2006; Ye et al., 2003).

RELATED WORK

Yung and Ye (1999) presented a new method for behavior based control for mobile robots path planning in unknown environments using fuzzy logic. The main idea of this paper is to incorporate fuzzy logic control with behavior-based control. The basic behaviors are designed based on fuzzy control technique and are integrated and coordinated to form complex robotics system. More behaviors can be added into the system as needed. The output from the target steering behavior and the obstacle avoidance behavior are combined to produce a heading which takes a robot towards its target location while avoiding obstacles. Player/Stage simulation results show that the proposed method can be efficiently applied to robot path planning in complex and unknown environments by fusing multiple behaviors and the fuzzy behaviors made the robot move intelligently and adapt to changes in its environment. Seng et al. (1999) demonstrated a successful way of structuring the navigation task in order to deal with the problem of mobile robot navigation. Issues of individual behavior design and action coordination of the behaviors were addressed using fuzzy logic. The coordination technique employed in this work consists of two layers. A layer of primitive basic behaviors, and the supervision layer which based on the context makes a decision as to which behavior(s) to Fuzzy Logic Based Navigation of Mobile Robots process (activate) rather than processing all behavior(s) and then blending the appropriate ones, as a result time and computational resources are saved. Simulation and experimental studies were done to validate the applicability of the proposed strategy. Yang et al. (2005) proposed an approach which utilizes a hybrid neuro-fuzzy method where the neural network effectively chooses the optimum number of activation rules time for real-time applications. Initially, a classical fuzzy logic controller has been constructed for the path planning problem. The inference engine required 625 if-then rules for its implementation. Then the neural network is implemented to choose the optimum number of the activation rules based on the input crisp values. Simulation experiments were conducted to test the performance of the developed controller and the results proved that the approach to be practical for real time applications. The proposed neuro-fuzzy optimization controller is evaluated subjectively and objectively with other fuzzy approaches and also the processing time is taken into consideration. Samsudin et al. (2011) dealt with the reactive control of an autonomous mobile robot

which should move safely in a crowded unknown environment to reach a desired goal. A successful way of structuring the navigation task in order to deal with the problem is within behavior based navigation approaches. In this study, issues of individual behavior design will be addressed using fuzzy logic approach. Simulation results show that the designed fuzzy controllers achieve effectively any movement control of the robot from its current position to its end motion without any collision. Wang and Liu (2008) proposed a new behavior-based fuzzy control method for mobile robot navigation. This method takes angular velocities of driving wheels as outputs of different behaviors. Fuzzy logic is used to implement the specific behaviors. In order to reduce the number of input variables, we introduced a limited number of intermediate variables to guarantee the consistency and completeness of the fuzzy rule bases. To verify the correctness and effectiveness of the proposed approach, simulation and experiments were performed. Seraji and Howard (2002) presented a simple fuzzy logic controller which involves searching target and path planning with obstacle avoidance. In this contest, fuzzy logic controllers are constructed for target searching behavior and obstacle avoidance behavior based on the distance and angle between the robot and the target as inputs for the first behavior and the distance between the robot and the nearest obstacle for the second behavior; then a third fusion behavior is developed to combine the outputs of the two behaviors to compute the speed of the mobile robot in order to fulfill its task properly. Simulation results show that the proposed approach is efficient and can be applied to the mobile robots moving in unknown environments. Selekwa et al. (2005) proposed navigation and obstacle avoidance in an unknown environment using hybrid neural network with fuzzy logic controller. The overall system is termed as Adaptive Neuro-Fuzzy Inference System (ANFIS). ANFIS combines the benefits of fuzzy logic and neural networks for the purpose of achieving robotic navigation task. Abdessemed et al. (2004) presented a Mamdani type minimum rule base fuzzy logic system which has been used successfully in a control system for robot hurdles avoidance in cluttered environment. The fuzzy logic will collect the sonar measurement data as inputs, and select an action for the robot so that it can navigate in the environment successfully.

Mobile robots have expected a substantial concentration from early research community, up to this instant. Today a fully automated robot is expected to travel, detect objects and explore any unknown environments. One such interest is focused on the predicament of generating a map for a functioning environment depiction for navigational tasks. A robot explores while travelling on a trajectory, with its sensors it senses the obstacles and generates a map. The most common sensors used are sonar and laser scanners, which detect the distance of an obstacle within the range

of the sensors by transmitting out signal and compute the time till the resonance of the signal income. The ultrasound rangefinders have a very wide possibility of exploitation due to their ease of functioning, low cost and modest realization. In the majority of circumstance the signal will bounce against the nearby obstacle in the course of the sensor and as a result the calculated distance will be the distance to the nearby obstacle. But however, there are some occasions where there occur measurement failures, and as a result the calculated distance becomes flawed. These measurement failures may occur due to the uncertainties provided by the range measuring sensors. These uncertainties are origin by the characteristics of air such as its temperature, humidity, turbulence and pressure.

One such ambiguity results from the promulgation of the ultrasonic signal to the space in the form of a cone with an axis in the scanning course. So the exact angular position of the object reflecting the echo might not be determined, because it may occur somewhere along the arc with the radius of the measured distance. A further cause of ambiguity is a experience of numerous reflections, that occurs in the case that the incidence angle of signal to the obstacle is larger than a so called critical angle, which is strongly reliant on the exterior distinctiveness. In this occurrence the reflection of the signal is mainly specular and the sensor may perhaps receive the ultrasonic beam after numerous reflections, what is called a elongated reading, or it may even get lost. Consequently, to return a momentous range reading, the angle of incidence on the object exterior has to be lesser than the critical angle.

Steering and obstacle evading are very significant issues for the doing well use of a sovereign mobile robot. Computing the configuration succession, allow the robot to move from one location to a further location. When the surroundings of the robot are obstacle free, the predicament becomes not as much of complex to handle. But as the surroundings becomes a complex, movement planning need much more effective to allow the robot to move between its in progress and closing configurations without any collision with the surroundings. A flourishing approach of configuring the steering assignment to deal with the dilemma is within behavior based navigation approaches.

The fundamental scheme in behavior based steering is to subdivide the navigation task into diminutive simple to supervise, course and sort out behaviors that focus on implementation of explicit sub schemes. For illustration, fundamental behaviors could be obstacle avoiding, target seeking, or wall following. This split and triumph over approach has turned out to be a flourishing approach, for it makes the scheme modular, which both make simpler the steering way out as well as tender a prospect to insert new behaviors to the system without causing any major increase in complexity.

The intention of this dissertation is to be evidence for

how to conduct an autonomous mobile robot in unfamiliar surroundings by means of fuzzy logic approach and to build map based on the range readings obtained from the sensors. Fuzzy logic control (FLC) is an appealing contrivance to be useful to the dilemma of conduit arrangement given that the output varies efficiently as the input adjusts. In this exertion, we will discuss a fuzzy conduit arrangement controller design based on connoisseur understanding and information that was applied to a mobile robot. The fuzzy inference system is based on a person driver reminiscent of interpretation in a indoor surroundings that is vacant or surround obstacles.

The paper is structured as follows: At first, the sculpt of the mobile robot is presented and the essential background of fuzzy logic method and a epigrammatic of fuzzy behavior based steering is presented. The proposed organizers, the map building algorithms are introduced and elucidated. Simulation results for illustration of movement of the robot in unknown surroundings are demonstrated.

DESIGN OF FUZZY BEHAVIOR BASED NAVIGATION METHOD

Mobile robot kinematics

In this exploration, a differentially ambitious mobile robot is used; its kinematic illustration is show in the Figure 1. The kinematic model of the mobile robot has two rear driving wheels and a passive front wheel. The inputs of the scheme are the steering angle α of the front wheel and the linear velocity V_R. The outputs are the coordinates of the robot (X_R, Y_R and θ_R). In ideal sticking together circumstances, this kinematic model can be described by the following equations:

$$X_R = V_R*\cos(\theta_R) \tag{1}$$

$$Y_R = V_R*\sin(\theta_R) \tag{2}$$

$$\theta_R = V_R * tg(\alpha)/l \tag{3}$$

Where X_R, Y_R are the position coordinates, θ_S angle error between the robot axis and goal vector and θ_R is the orientation angle of the robot. l is the robot length. In our work, we suppose that the simulated mobile robot is able to detect the coordinates of the final goal and it is equipped by sensors for perceiving its environment.

Fuzzy logic approach

The premise of fuzzy logic scheme is motivated by the significant human ability to rationale with perception based information. Rule based fuzzy logic afford a proper methodology for linguistic rules ensuing from interpretation and decision making with ambiguous and indefinite information. The building block illustration of a fuzzy control scheme is shown in Figure 2. The fuzzy controller is composed of fuzzification interface, a rule base, an interface mechanism. The fuzzification interface renovates the actual controller inputs into information so as to the inference mechanism can straightforwardly exercise to make active and relate rules. A rule-base has a set of If-Then rules which enclose a fuzzy logic quantification of the connoisseur's linguistic depiction of how to
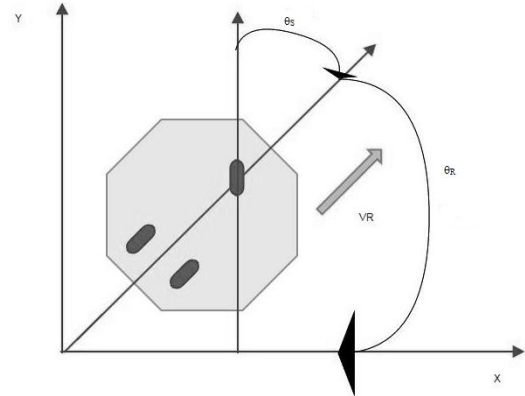
Figure 1. Mobile robot kinematics.

accomplish superior control. An inference mechanism emulates the connoisseur's decision making in interpreting and concern understanding about how preeminent to direct the plant. defuzzification interface renovate the conclusions of the inference mechanism into actual inputs for steering the course. Mamdani and Takagi-Sugeno model are two popular models used mostly in fuzzy logic control. In this paper we use zero order Takagi-Sugeno model owing to its simplicity and effectiveness to the course control.

Design of robot steering and velocity control

The motion control variables of the mobile robot are the angular velocity of the front wheel and the velocity of the rear wheels. The angular velocity is represented by θ_R. The vehicle velocity is determined by the rear wheels speed which is denoted by V_R. The position of the vehicle is denoted by (X_R, Y_R).

The left steering angle is represented by a three-variable linguistic fuzzy input membership set {S, LO1, LO2} which define the distance of the obstacles in three different levels from farthest to the closet respectively, the obstacle distances are estimated from the ultrasound sensor range readings, and the output membership set {ST, L1, L2} which define the steering actions to the left of the vehicle in the different levels from straight steering to intense left turning actions respectively.

Similarly the right steering angle is represented by a three-variable linguistic fuzzy input membership set {S, RO1, RO2} which define the distance of the obstacles in three different levels from farthest to the closet respectively, and the output membership set {ST, R1, R2} which define the steering actions to the right of the vehicle in the different levels from straight steering to intense left turning actions respectively. The rule base of the steering behavior is summarized in Table 1.

Similarly the motor speed of the rear wheel is represented by a five-variable linguistic fuzzy input membership set {D1, D2, D3, D4, D5}, defines the five different levels of obstacle distance from the front end of the mobile robot from very near to the farthest position respectively and the output membership {V1, V2, V3, V4, V5} which define the velocity actions such as too slow, slow, medium, fast, fastest most respectively.

Design of goal seeking behavior

The mission of the robot is to arrive at a preferred position in the surroundings called a goal. This goal seeking behavior is anticipated to line up the robot's cranium with the course of the goal
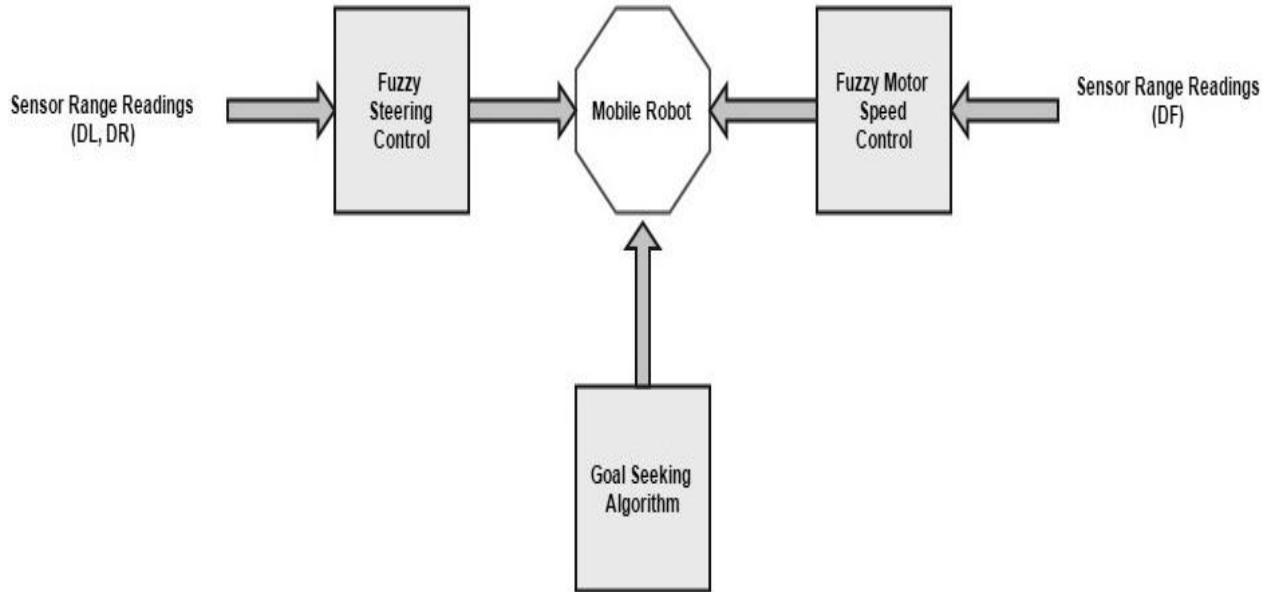
Figure 2. Block Diagram of the proposed scheme.

Table 1. Fuzzy rule set.

Fuzzy rule base for steering control	Fuzzy rule base for motor control
1. If (input1 is LO2) then (output1 is L2)	1. If (input1 is D1) then (output1 is V1)
2. If (input1 is LO1) then (output1 is L1)	2. If (input1 is D2) then (output1 is V2)
3. If (input1 is S) then (output1 is ST)	3. If (input1 is D3) then (output1 is V3)
	4. If (input1 is D4) then (output1 is V4)
1. If (input1 is RO2) then (output1 is R2)	5. If (input1 is D5) then (output1 is V5)
2. If (input1 is RO2) then (output1 is R1)	
3. If (input1 is S) then (output1 is ST)	

coordinates. The calculation module compares the actual robot coordinates with the coordinates of the target using mathematical equations. The outputs are the angle noted θ_D and the distance between the robot and the goal (position error) noted D_{RG}. The angle value is compared with the orientation of the robot delivered by the odometry module in order to compute the angle error θ_{ER} between the robot axis and the goal vector. Prearranged a mobile robot, it must be capable to engender a course between two specific position, the start nodule and the target nodule. The course ought to be free of collision and be required to persuade convinced optimization criterion i.e. least time consuming course. The only information offered to the robot is it's in progress location and the location of the goal in the grid map. The robot has to constantly be in motion from the in progress position until it reaches the goal by avoiding the obstacles detected on course. Occupancy grids are used for the representation of the environment.

At this juncture each cell in the grid encloses information concerning its circumstances, which is premeditated depending on the probability of occupancy of that particular cell. Consequently a cell which is engaged by an obstacle will cover a very high probability of occupancy cost returned by the sensor, which makes it engaged for the robot to pass through. Frontier based heuristic exploration algorithm is the chief province of the dilemma. It is

helpful in situations wherever no preceding preparation is viable and all decisions are taken at instantaneous.

To begin with the robot executes a bursting surrounding look into of its surroundings and updates the occupancy cost G_O of its four neighboring cells, one in each course: top, right, bottom and left. These four cells sensed on each scan are termed as the cells in the in progress sensing area. A frontier cell is a cell explored by the robot which is having at least one unexplored cell as its neighboring cell. After each scanning operation, the newly detected frontier cells are assigned heuristic cost value known as Goal Seeking Index $G_{SI}(X_R, Y_R)$. The cost of moving to a cell (X_R, Y_R) is found as the product of its occupancy cost G_O and the distance of the cell (X_R, Y_R) from the in progress position of the robot. Calculating the cost based on occupancy value is explained well in the GSI for each frontier cell is found out with the help of Equation (4):

$$G_{SI}(X_R, Y_R) = ((D_{MAXIMUM} - D_{((X,Y),TARGET)}) - C_{((X,Y),CURRENT)}) \qquad (4)$$

Where $D_{MAXIMUM}$ is the principal distance probable amid any cell in the grid and the goal location, $D_{((X,Y),TARGET)}$ is the distance amid the given frontier cell (X_R, Y_R) and the goal cell, and $C_{((X,Y),CURRENT)}$ is product of the occupancy cost (G_O) of the frontier cell (X_R, Y_R) and its distance from the current location of the robot.

Table 2. Simulation parameters.

Specification	Description
Operating System	Windows Seven
Simulation Tool	MATLAB 2009
Number of Robots	1
Simulation Area	50m x 50m
No of wheels	3 (2 Rear + 1 front steering)
Minimum – Maximum Motor Speed	0-30 RPM
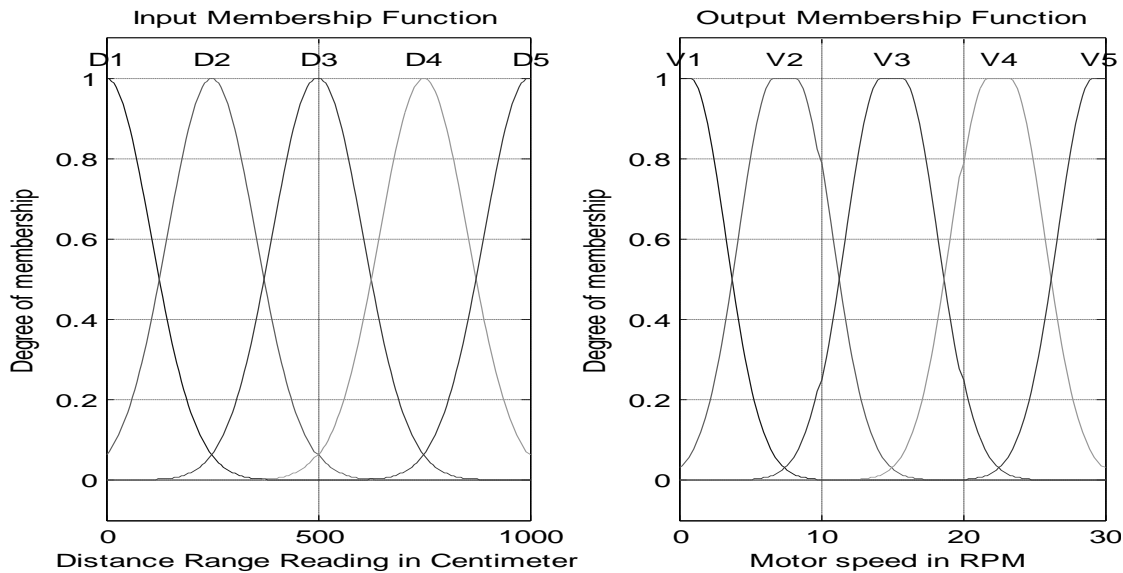
Figure 3. Input and output membership function for Motor speed control.

RESULTS AND DISCUSSION

For the proposed scheme, simulation has been done with MATLAB. The simulation parameters are described in Table 2. Figure 3 shows a five-variable linguistic fuzzy input membership set {D1, D2, D3, D4, D5}, defines the five different levels of obstacle distance from the front end of the mobile robot from very near to the farthest position respectively and the output membership {V1, V2, V3, V4, V5} which define the velocity actions such as too slow, slow, medium, fast, fastest most respectively. Figure 4 shows the left steering angle which is represented by a three-variable linguistic fuzzy input membership set {S, LO1, LO2} which define the distance of the obstacles in three different levels from farthest to the closet respectively, the obstacle distances are estimated from the ultrasound sensor range readings, and the output membership set {ST, L1, L2} which define the steering actions to the left of the vehicle in the different levels from straight steering to intense left turning actions respectively. Similarly the right steering

angle is represented by a three-variable linguistic fuzzy input membership set {S, RO1, RO2} which define the distance of the obstacles in three different levels from farthest to the closet respectively, and the output membership set {ST, R1, R2} which define the steering actions to the right of the vehicle in the different levels from straight steering to intense left turning actions respectively. Figure 5 shows the robot steering control achieved in turn angle with respect to the distance of the obstacle sensed in the left and right of the robot. Figure 6 shows the robot speed control achieved in rotations per minute with respect to the obstacle distance sensed by the front sensor range readings. Figures 7, 8 and 9 shows the robot goal seeking in a MATLAB simulated environment with a high obstacle density similar to a maze like environment. Here, the robot is supposed to move from the start point $(X_I, Y_I) = (45, 45)$ to the goal $(X_T, Y_T) = (5, 5)$ in two different environments. The initial orientation of the robot is $\theta m = \pi/2$ and there are many obstacles in the environment. The obtained results show the efficiency of the proposed control method. In all the
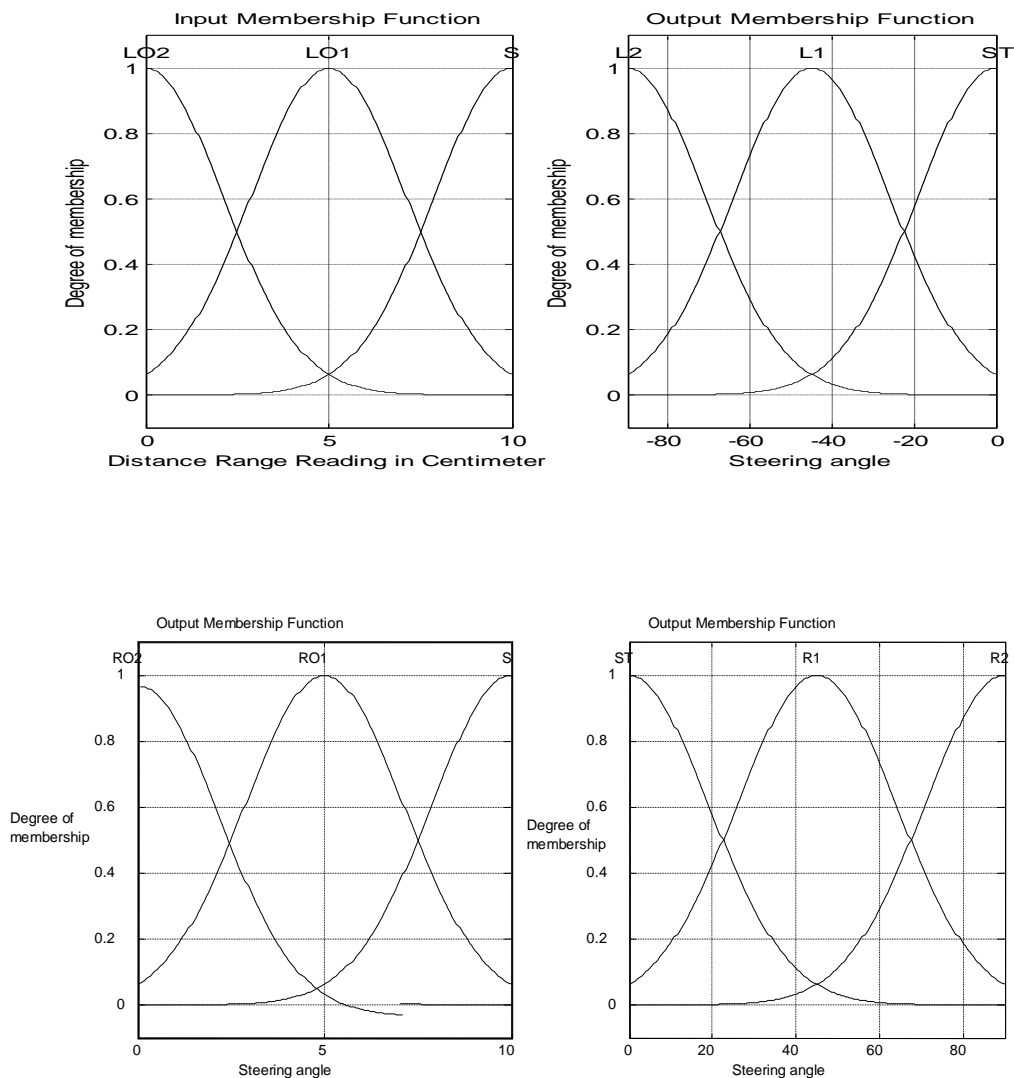
Figure 4. Input and output membership function for motor steering control.
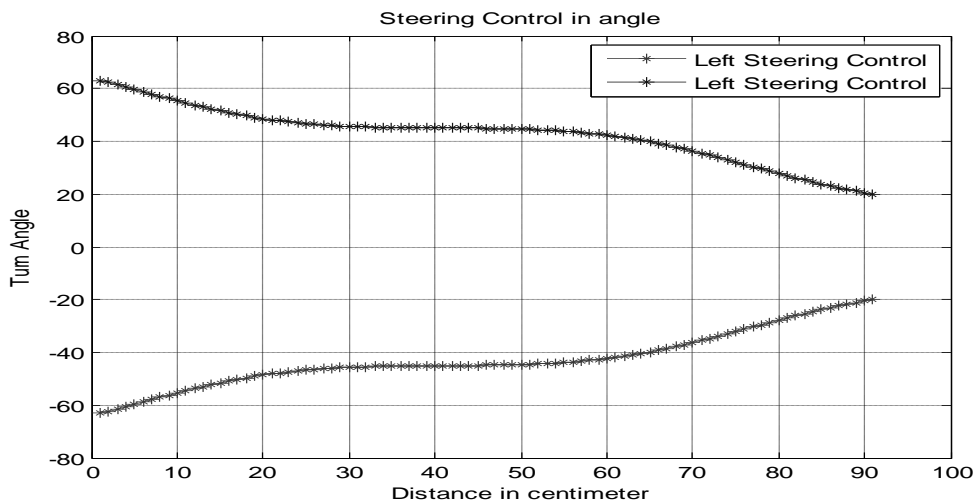
Figure 5. Robot steering control distance vs. turn angle.
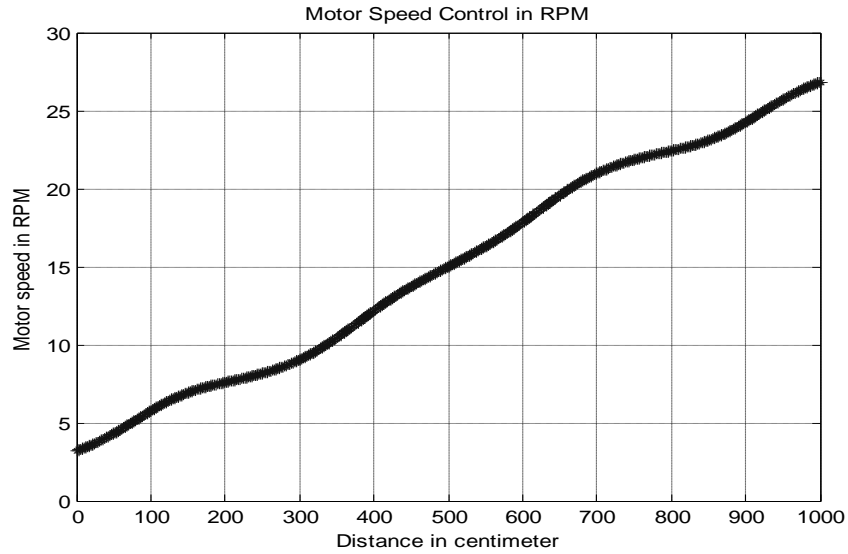
Figure 6. Robot speed control distance vs. motor speed in RPM.
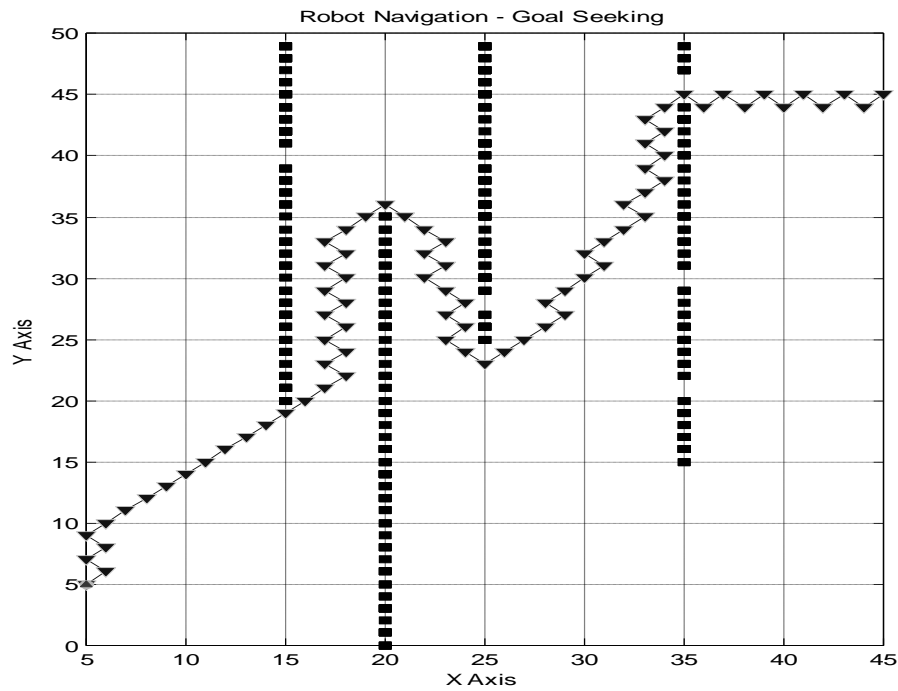
Figure 7. Robot goal seeking in Environment 1.

different configuration of the environment, the robot is able to reach the goal point.

CONCLUSION

This work presented a method that can be efficiently used to design behaviors based steering scheme. An uncomplicated harmonization scheme is used to toggle between steering procedures according to outputs of apiece manners. The outcome attained illustrates the effectiveness of the proposed control scheme. In every scenario, the robot is capable to arrive at the goal in diverse configurations of the surroundings by avoiding

Robot Navigation - Goal Seeking
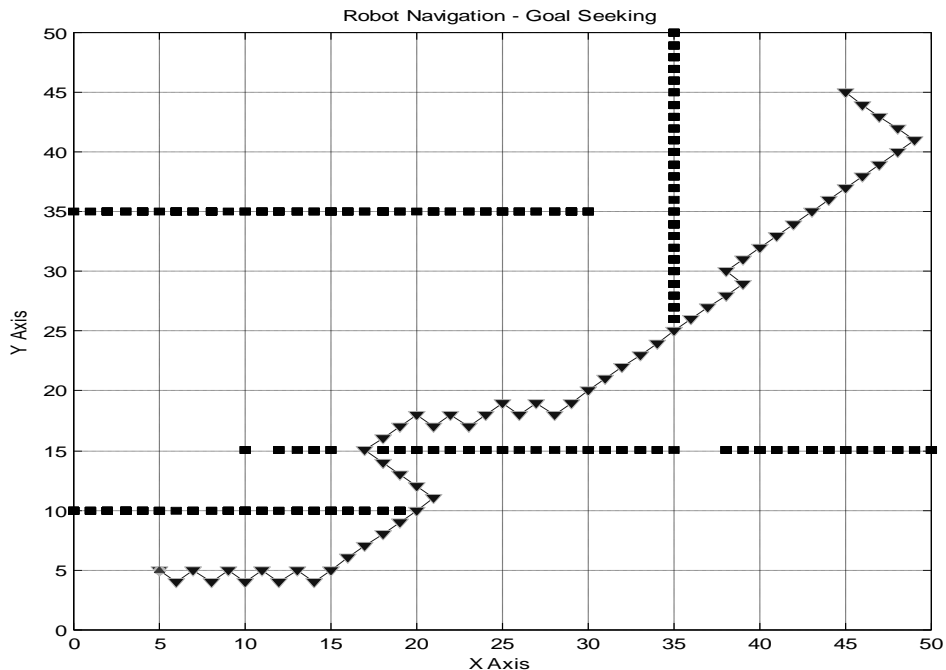
Figure 8. Robot goal seeking in Environment 2.

Robot Navigation - Goal Seeking
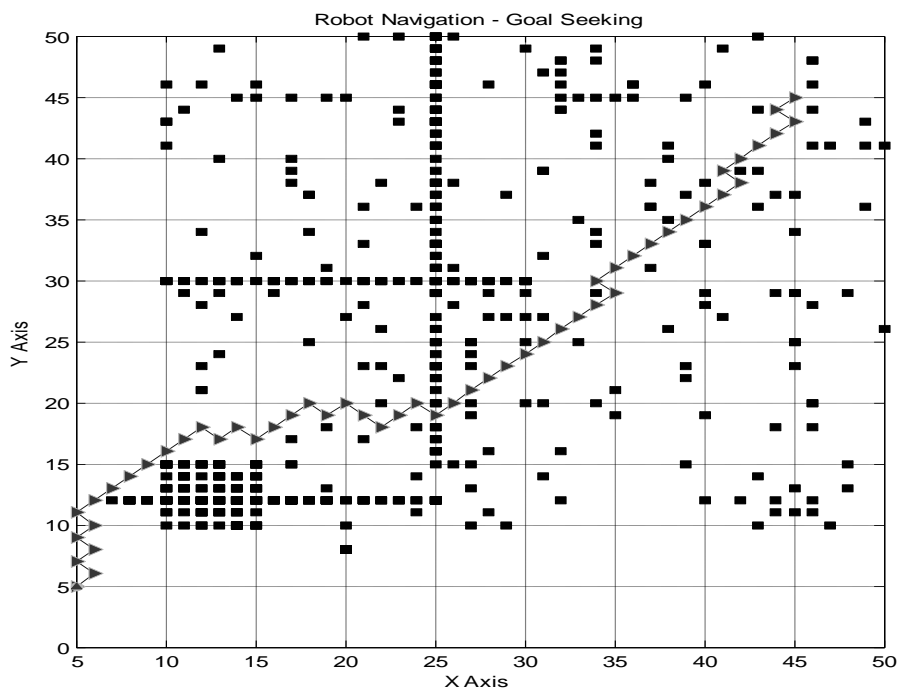
Figure 9. Robot goal seeking in Environment 3.

obstacles. It is of an immense significance to highlight on the attained efficiency of the robot activities. In prospect the attention will be certain to the development of an inclusive steering scheme counting other behaviors like wall following and avoiding moving obstacles. In future works, the interest will be given to moving obstacles.

Conflict of Interest

The authors have not declared any conflict of interest.

REFERENCES

Abdessemed F, Benmahammed K, Monacelli E (2004). A fuzzy based reactive controller for a non-holonomic mobile robot. Robotics and Autonomous Systems. 47(1):31–46.

Beom HR, Cho HS (1995). A sensor-based navigation for a mobile robot using fuzzy Logic and Reinforcement Learning. IEEE Tran. Syst. Man. Cyber. 25(3):464-477.

Brooks RA (1989). A Robot that Walks; Emergent Behavior from a Carefully Evolved Network. IEEE International Conference on Robotics and Automation. Scottsdale; AZ. pp. 292–296.

Brooks RA (1986). A Robust Layered Control System for a Mobile Robot. IEEE J. Robotics Autom. RA-2(1):14–23.

Ehsan H, Maani GJ, Navid GJ (2011). Model based PI-fuzzy control of four-wheeled omni-directional mobile robots. Robot. Autom. Syst. 59(11):930-942.

Fatmi AS, Yahmedi AI, Khriji L, Masmoudi N (2006). A Fuzzy Logic based Navigation of a Mobile robot. World academy Sci. Eng. Technol. 22:169-174.

Janglova D (2004). Neural networks in mobile robot motion. Int. J. Adv. Robot. Syst. 1(1):15-22.

Kian HL, Wee KL, Jr. Ang MH (2002). Integrated planning and control of mobile robot with self-organizing neural network. Proceeding of18th International Conference onRobotics and Automation (ICRA '02). May 11-15, 4:3870-3875.

Saffiotti A (1997). The uses of fuzzy logic for autonomous robot navigation. Soft Comput. 1(4):180-197.

Samsudin KF, Ahmad A, Mashohor S (2011). A highly interpretable fuzzy rule base using ordinal structure for obstacle avoidance of mobile robot. Appl. Soft Computing J. 11(2):1631–1637.

Selekwa MF, Damion D, Collins Jr. EG (2005). Implementation of multi-valued fuzzy behavior control for robot navigation in cluttered environments. Proceedings of the 2005 IEEE International Conference on Robotics and Automation, Barcelona, Spain. pp. 3699-3706.

Seng TL, Khalid MB, Yusof R (1999). Tuning a Neuro-Fuzzy Controller by Genetic Algorithm. IEEE Trans. Syst. Man. Cybernetics 29(2):226-236.

Seraji H, Howard A (2002). Behavior - based robot navigation on challenging Terrain: A Fuzzy Logic Approach. IEEE Trans. Rob. Autom. 18(3):308-321.

Shuzhi SG, Lewis FL (2006). Autonomous Mobile Robots, Sensing, Control, Decision, Making and Applications, CRC, Taylor and Francis Group.

Sugihara K, Smith J (1997). Genetic algorithms for adaptive motion planning of an autonomous mobile robot. Proceedings of the IEEE International Symposium on Computational Intelligence in Robotics and Automation. pp.138-146.

Velappa G, Soh CY, Jefry Ng (2009). Fuzzy and neural controllers for acute obstacle avoidance in mobile robot navigation. IEEE/ASME International Conference on Advanced Intelligent Mechatronics Suntec Convention and Exhibition Center. pp.1236-1241.

Wang M, Liu JNK (2008). Fuzzy logic-based real-time robot navigation in unknown environment with dead ends. Robotics Autonomous Syst. 56(7):625–643.

Yang SX, Moallem M, Patel RV (2005). A layered goal-oriented fuzzy motion planning strategy for mobile robot navigation. IEEE transactions on systems, man, and cybernetics—part b: cybernetics. 35(6):1214-1224.

Ye CN, Yung HC, Wang D (2003). A fuzzy controller with supervised learning assisted reinforcement learning algorithm for obstacle avoidance. IEEE Trans. Syst. Man. Cybern. B. 33(1):17-27.

Yung NHC, Ye C (1999). An intelligent mobile vehicle navigator based on fuzzy logic and reinforcement learning. IEEE Trans. Syst. Man. Cybern. 29(2):314-321.

Full Length Research Paper

Multi-objective optimization of hybrid PV/wind/diesel/battery systems for decentralized application by minimizing the levelized cost of energy and the CO$_2$ emissions

B. Ould Bilal[1]*, D. Nourou[3], C. M. F Kébé[2], V. Sambou[2], P. A. Ndiaye[2] and M. Ndongo[3]

[1]Ecole des Mines de Mauritanie (EMiM), BP : 5259 Nouakchott-Mauritanie, Sénégal.
[2]Centre International de Formation et de Recherche en Energie Solaire (C.I.F.R.E.S), ESP-UCAD, BP: 5085 Dakar Fann Sénégal.
[3]Laboratoire de Recherche Appliquée aux Energies Renouvelables de l'eau et du froid (LRAER), FST- Université des Sciences de Technologies et de Médecines (USMT), BP: 5026 Nouakchott-Mauritanie, Sénégal.

The main objective of this paper is to propose a methodology to design and optimize a stand-alone hybrid PV/wind/diesel/battery minimizing the Levelized Cost of Energy (LCE) and the CO$_2$ emission using a Multi-Objectives Genetic Algorithm approach. The methodology developed was applied using the solar radiation, temperature and the wind speed collected on the site of Potou located in the northwestern coast of Senegal. The LCE and the CO$_2$ emission were computed for each solution and the results were presented as a Pareto front between LCE and the CO$_2$ emission. These results show that as the LCE increases the CO$_2$ emission decreases. For example, the solution A (left solution on the Pareto front) presents 2.05 €/kWh and 11.89 kgCO$_2$/year, however the solution E (right solution on the Pareto front) shows 0.77 €/kWh and 10,839.55 kgCO$_2$ /year. It was also noted that the only PV/battery or Wind/ battery was not an optimal configuration for this application on the site of Potou with the use of the load profile and the specifications of the used devices. For all solutions, the PV generator was more adapted to supply the energy demand than the wind turbines.

Key words: Hybrid system, optimization, genetic algorithm, cost of energy, CO$_2$ emission.

INTRODUCTION

The scarcity of conventional energy resources, the rise in the fuel prices and the harmful emissions from the burning of fossil fuels has made power generation from conventional energy sources unsustainable and unviable.

It is estimated that this supply demand gap will continue to rise exponentially unless it is met by some other means of power generation. Further, inaccessibility of the grid power to the remote places and the lack of rural

electrification have prompted to use other sources of energy (Prabodh and Vaishalee, 2012). In the remote regions, far from the grids, electric energy is usually supplied using diesel generators. In most of cases, supplying demand energy using diesel fuel is so expensive and increases the amount of CO_2 emitted. So, renewable energy resources (e.g. solar and wind energies) have become the better alternatives for conventional energy resources. However, the use of a single renewable energy source such as wind energy or solar energy is not adequate to meet the demand for long periods due to the intermittent nature of the renewable energy high, the cost of system as well as storage subsystem (Ayong et al., 2013; Bekele and Palm, 2010; Diaf et al., 2008 ; Ekren-O and Ekren- by, 2010; Kalantar and Mousavi, 2010; Kanase-Patil et al., 2011; Saheb-Koussa et al., 2009; Zhou et al., 2010). To meet this challenge, the renewable sources such as wind and solar energy can be used in combination with the conventional energy systems making a hybrid PV/wind/diesel/battery system. These kinds of systems could allow dropping the investment, operation and the maintenance costs of systems (Colle et al., 2004).

Hongxing et al. (2009); Kyoung-Jun et al. (2013); Mukhtaruddin et al. (2015) have designed PV/wind hybrid systems coupled or now to battery bank and diesel generator by using different methods. A performance and feasibly study of hybrid renewable hybrid system coupled to batteries was done in the work of Kyoung-Jun et al. (2013); Ajay et al. (2011); Suresh-Kumar and Manoharan (2014) and Ismail et al. (2014, 2013). However, in the most case, the system was PV/diesel, PV/wind or PV/wind/batteries system. Also, in these studies, the type of devices was not taking into account in the optimization.

Several others studies on the feasibility, performance, and economic viability of hybrid power systems have been conducted using Homer (Hybrid Optimization Modeling Software) in the works of Chong et al. (2013); Bahtiyar (2012); Mir-Akbar et al. (2011); Sanjoy and Himangshu (2009); Patrick et al. (2014); Ahmad et al. (2010); Rohit and Subhes (2014); Ahmed et al. (2011); Zeinab et al. (2012); Mei and Chee (2012); Dalton et al. (2009); Belgin and Ali (2011); Eyad (2009); Alam and Manfred (2010) and Muyiwa et al. (2014). With the use of Homer, the best hybrid renewable energy configuration is which have the lower cost. However, Homer does not take into account the number of components such as variable. Also, Homer uses the monthly meteorological data variation (solar and wind speed). With the hourly solar and wind speed variation, the configuration chosen is more adapted to supply the demand.

Iterative methods of optimization have used to minimize the Annualized Cost of System (ACS) (Yang et al., 2008, 2007, 2003; Yang and Lu, 2004; Diaf et al., 2008; Shen, 2009; Kellogg et al., 1998; Koutroulis et al., 2006). These methods made possible to study the optimization

and the performance of a hybrid system. In the works of Duffo-Lopes and Bernal- Agustin (2005, 2008); Senjyu et al. (2007); Ekren and Ekren (2008) and Hongxing et al. (2009), authors have studied the performance of hybrid systems using genetic algorithms minimizing the cost of the system. The methods outlined in these works did not take into account all devices of the system such as wind turbine, PV module, regulator, battery, inverter and diesel generator. Ould Bilal et al. (2010) have designed and optimized hybrid PV/wind/battery systems minimizing the ACS and the Loss of Power Supply Probability (LPSP). The authors did not take into account the diesel generator. So, the CO_2 emission was not evaluated. Since the presented problem is a Multi-objective Optimization Problem (MOP), it requires a multi-objective method for solving. This paper utilizes a Pareto-based approach which can obtain a set of optimal solutions instead of only one (Mohammad et al., 2014). The objectives to be minimized in this paper are the levelized cost of energy and the CO_2 emission.

The developed methodology was applied using the solar radiation, temperature and the wind speed collected in the site of Potou located in the northwestern coast of Senegal. The decision variables included in the optimization process are the number of PV modules, the number of wind turbines, the number of batteries, the number of regulators, the number of inverters, the number of diesel generators and the type of each device.

APPROACH AND METHODOLOGY

Hybrid solar-wind-diesel power generation system coupled to the battery bank consists of a PV module, wind turbine, diesel generator, regulator, battery bank and an inverter. A schematic diagram of the basic hybrid system is shown in Figure 1. The PV module and the wind turbine work together to meet the load demand. When the energy sources (solar and wind energy) are sufficient, the generated power, after meeting the load demand, provides energy to the battery up to its full charge. The battery supplies energy demand to help the system to cover the load requirements, when energy from renewable energy is inferior to the load demand. The load will be supplied by diesel generators when power generation by both wind turbine and PV array is insufficient and the storage is depleted. The mathematical model of the components used in this study are detailed by the Ould Bilal et al. (2012a, b).

In this paper, the Levelized Cost of consumed Energy (LCE) was considered. We do not consider the cost of the energy generating because, in the remote village, most of the energy generated was lost. For example, if the PV generator or wind turbine generator produces energy during an hour when the electrical load is zero and the batteries are fully charged, then the energy produced was lost. In addition to that, the energy is also lost in the charge and discharge processes of the batteries.

OBJECTIVE FUNCTIONS

The objectives function to be minimized is the LCE and the pollutant emission (kg of CO_2 which is the main cause of the
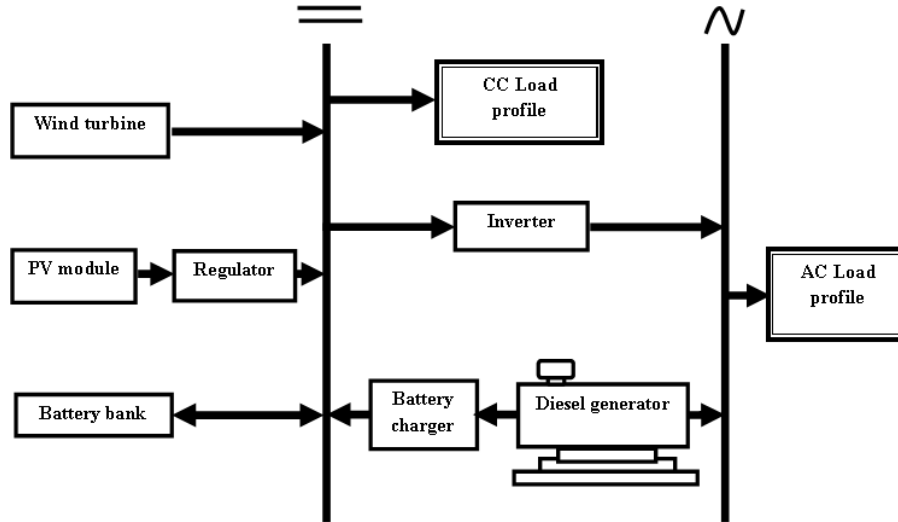
Figure 1. Bloc diagram of the hybrid solar/wind/diesel/battery system.

greenhouse effect).

Economic model based on LCE concept

The optimal combination of a hybrid solar-wind-diesel-batteries system can make the best compromise between the system pollutant emission and the total cost of energy. The economical approach, according to the concept of LCE is developed to be the best benchmark of system cost analysis in this study. According to the studied system, the LCE is composed of the capital levelized cost C_{acap}, maintenance and operation levelized cost C_{amain} and the replacement levelized cost C_{arep}.

Six devices of the hybrid system were considered: PV module, wind turbine, diesel generator, battery, regulator and inverter. The levelized cost of the kWh/year is defined as in Equation (1).

$$\mathrm{ACE} = \frac{\mathrm{J(x)}}{\mathrm{E_{annual}}} \tag{1}$$

$J(x)$ is the levelized cost of energy given by Equation (2).

$$\mathbf{J(x)} = \mathbf{C_{acap}(x)} + \mathbf{C_{amain}(x)} + \mathbf{C_{arep}(x)} \tag{2}$$

Where E_{annual} is the annual consumed energy (kWh/year), $x=[N_{pv},N_{ag},N_{dg},N_{rg},N_{bt},\ N_{inv,pv},T_{pv},\ T_{ag},T_{dg},T_{bt},T_{rg},T_{in}]$ is the decision vector of variables. Where T_{pv}, T_{ag}, T_{dg}, T_{bt}, T_{rg}, T_{in} are the types of PV module, wind turbine, diesel generators, batteries, solar regulators and inverters. C_{acap}, C_{amain} and C_{arap} are the levelized capital cost, levelized maintenance cost and the levelized replacement cost.

Pollutant emissions

The parameter considered in this paper to measure the pollutant emission is the (kg of CO_2). It represents the large percentage of the emission of fuel combustion (Sonntag et al., 2002). Further, CO_2 represents the main cause of the greenhouse effect. So, we evaluate the amount of the CO_2 produced by the diesel generator in

the PV/wind/ diesel/battery system. The fuel consumption of the diesel generator depends on the output power. It is given by Equation (3).

$$\mathbf{Cons} = \mathbf{B \cdot P_{NG}} + \mathbf{A \cdot P_{OG}} \tag{3}$$

A=0.246 l/kWh and B=0.08145 l/kWh are the coefficient of the consumption curve, defined by the user in (l/kWh) (Belfkira et al., 2011). The factor considered in this work to assess the emission of CO_2 was 3.15 kgCO_2/l (Fleck and Huot, 2009).

System optimization model using multi-objectives genetic algorithm

The main objective of this work is to design and optimize hybrid PV/wind/diesel/battery systems by minimizing the LCE and the CO_2 emission. These objectives are antagonist e.g. the increase of the LCE implies the decrease of the CO_2 emission and vice versa. So, it is important to find an efficient way to solve this Multi-Objective Problem (MOP) which parameters are also independent. The Multi-Objective Genetic Algorithm, which has the important characteristics of the concept of optimal Pareto front (Coello et al., 2002) can be used to solve this problem. A Pareto front is a set of a possible solution obtained after a search process.

The Multi-Objective function used in this study was implemented by employing genetic algorithm (GA) developed by Leyland and Molyneaux (Leyland, 2002; Molyneaux, 2002). This tool was designed for the optimization of the engineering energy systems. That is generally non-linear and uses a statistical technique of grouping of the individual basis on the independent variable (creation of the families which evolves in independent manner). This method has the advantage of maintaining the diversity of the population and making coverage the algorithm towards optima even difficult to find (Sambou, 2008).

Multi-objective solution strategy

Multi-objective problem (MOP) refers to the simultaneous optimization of multiple conflicting objectives, which produces a set

of solutions instead of one particular solution while some constraints should be met. In fact, most of time, we find a set of solutions, owning to the contradictory objectives. MOP can be formulated (Mohammad et al., 2013 ; Azizipanah-Abarghooee et al., 2012; Anvari Moghaddam et al., 2011) as:

$$\mathbf{Minimize\,F(X)} = \left(F_1(X), F_2(X), ..., F_{Nobj}(X)\right)$$

(4)

Subject to $u_i(X) < 0$, i=1, 2,…, H and $v_i(X) < 0$, i=1, 2,..., H
Where, Fi is the ith objective function, X is a determination vector that presents a solution, N_{obj} is the number of objectives. L and H are the number of the equality and the inequality constraints, respectively. In our cas $N_{obj} = 2$.

Operation system strategy

The PV generator and the wind turbine outputs are calculated according to the PV modules and the wind turbine system model by using the specifications of the PV module and the wind turbine as well as the solar radiation, the temperature and the wind speed data. The battery bank with the total nominal capacity φ_r is permitted to discharge up to a limit defined by the minimum state of charge. For a good knowledge of the real state of charge (SOC) of a battery, it is necessary to know the initial SOC, the charge or discharge time and the current. However, most storage systems are not ideal, losses occur during charging and discharging and also during storing periods (Hongxing et al., 2009). Taking these factors into account, the SOC of the battery at time t + 1 can be calculated by Equation (5).

$$SOC(t+1) = SOC(t) \cdot \left(1 - \frac{\sigma \cdot \Delta t}{24}\right) + \eta_{bt} \cdot \frac{P_{bt}(t) \cdot \Delta t}{U_{bt} \cdot \varphi_{bt}}$$

(5)

Where σ is the self-discharge rate which depends on the accumulated charge and the battery state of health (Guasch and Silvestre, 2003) and a proposed value of 0.2% per day is recommended, η_{bt} is the battery charging and discharging efficiency. It is difficult to measure separate charging and discharging efficiency, so manufacturers usually specify roundtrip efficiency. In this paper, the batteries charge efficiency is set equal to 80%, and the discharge efficiency is set equal to 100% (Duffos Lopes et al., 2005). U_{bt} (V) is the nominal batteries voltage, which is equal to the nominal system operating voltage and P_{bt} (t) is the power received by the battery from generators or requested by the demand. The minimum state of charge of the battery bank (SOC$_{min}$) can be expressed by Equation (6).

$$SOC_{min} = (1 - DOD) \cdot SOC_r$$

(6)

Were DOD (%) is the depth of discharge and SOC$_r$ is the rated state of charge of the battery bank. In our case, the DOD assumed equal to 60%. So, the minimum state of charge (SOC$_{min}$) that the battery bank can achieve is of 40% SOC$_r$.
The input/output battery bank power can be computed according to the following strategy:

(i) If $PT(t) = \frac{P_{ch}(t)}{n_{ond}}$, all the produced energy is consumed by the demand. So P$_{bt}$(t)=0

(ii) If $PT(t) > \frac{P_{ch}(t)}{n_{ond}}$, then the surplus of power $P_{bt}(t) = PT(t) - \frac{P_{ch}(t)}{n_{ond}}$

is used to charge the battery. The new battery state of charge is then calculated by using the Equation (5)

(iii) if $PT(t) < \frac{P_{ch}(t)}{n_{ond}}$, then the lack of power $P_{bt}(t) = PT(t) - \frac{P_{ch}(t)}{n_{ond}}$ is provided by the battery. The new battery state of charge is calculated by using the Equation (5).

(iv) if $PT(t) < \frac{P_{ch}(t)}{n_{ond}}$ and the battery bank are depleted (SOC=SOC$_{min}$) or the energy providing from the battery bank is not enough to supply the load, then the diesel generators supply needed by the load and the surplus energy (if any), is used to charge the battery bank (Gupta et al., 2011). PT (t) is he total output power of the wind turbine and PV module generators (Ould Bilal et al., 2012a, b). The initial assumption of system configuration will be a subject to the following inequalities constraints:

$$\begin{cases} SOC_{min} \leq SOC \leq SOC_{max} = SOC_r \\ I_{max} \leq I_{rrg} \\ P_{max} \leq P_{rond} \end{cases}$$

(7)

Where: SOC$_{min}$ and SOC$_{max}$ are the minimum and the maximum of the state of charge of the battery bank, I$_{max}$ is the maximum current delivered by the PV generated, I$_{rrg}$ is the nominal current of the designed regulators (A), P$_{max}$ is the maximum power of the demand and P$_{rond}$ is the nominal power of the inverter (W).

Application on the site of Potou in Senegal

Presentation of the site

The methodology developed was applied using the solar radiation, the temperature and the wind speed collected for eight month on the site of Potou (16.27° of longitude West, 14.3° of latitude North and 21 m of altitude) located in the Northwestern coast of Senegal. This region is characterized by a wind potential adapted to small wind turbines (about 0. 2 to 10 kW) on the one side and on the other side, this region is characterized by a very sunny weather which can be used to produce energy with the use of PV module.

In this area an anemometer, a pyranometer and temperature sensor have been installed to collect the solar radiation, temperature and the wind speed. A data acquisition system was used to record the parameters every one second. Then, the data are averaged over 10 min intervals and was recorded in the memory of the datalogger. The used data were averaged over each one hour. Results presenting the real distribution and the theoretical distribution of Weibull of the mean wind speed are shown in Figure 2. Figure 3 shows the hourly radiation for a typical day on the site of Potou. The wind power density and the solar energy are 95 W/m² and 3.90 kWh/m²/d respectively.

Load profile

The daily load profile is represented by a sequence of powers and it is considered as constant over a time-step of 1 h. The used load profile (Figure 4) denotes the consumption of a typical isolated town which fluctuation during the day corresponds to the operation of public and domestic equipments (refrigerators, television, radio, domestic mill, welding machines, sewing machine and other equipment). The peak of demand observed at night corresponds to the use of the domestic equipment (refrigerators, lighting, television, radio) and some commercial equipment (refrigerator and lighting in
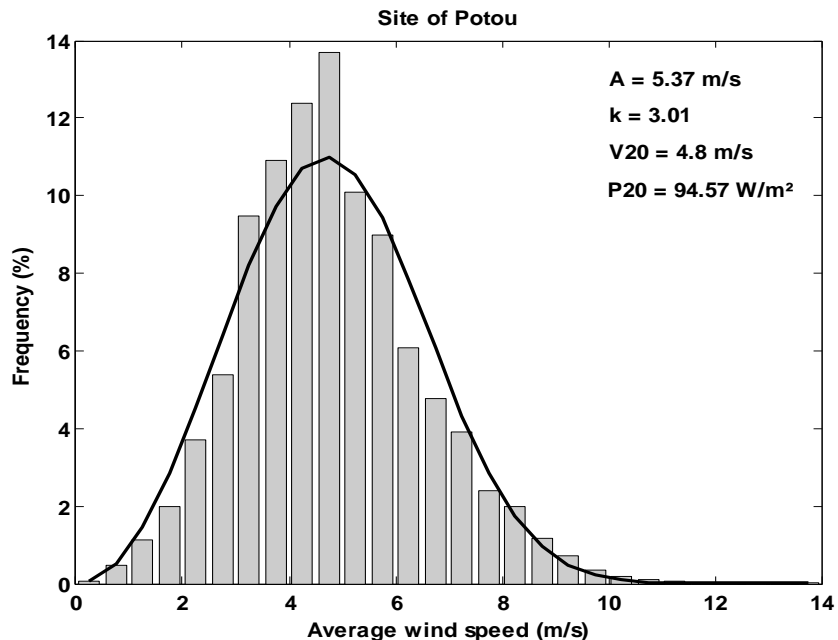
Figure 2. Real distribution and Weibull distribution on the site of Potou.
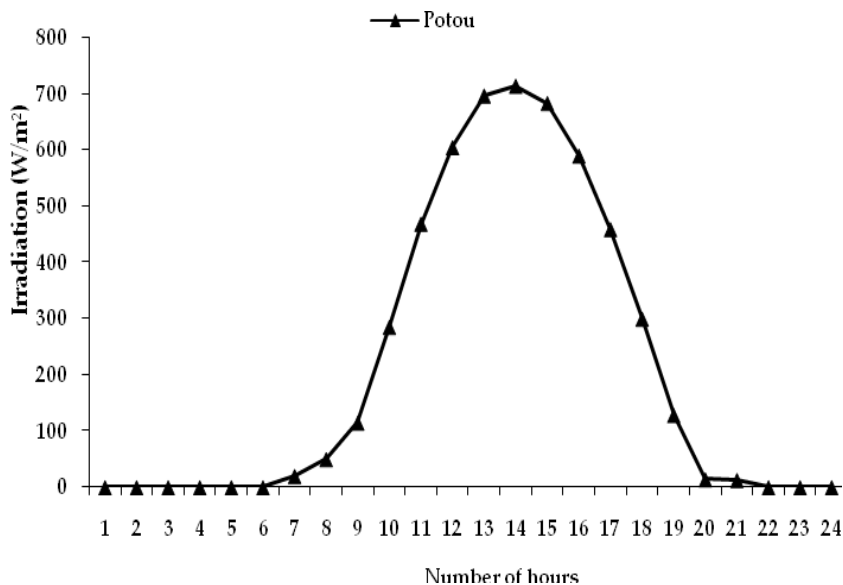
Figure 3. Solar Irradiation profile on the site of Potou.

the shops). The light and the television are the main element used overnight in the remote village. The total consumption energy of the used load profile is 94 kWh/d.

Components characteristics

The specifications of the components used to design and optimize hybrid PV/wind/diesel/battery are presented in Table 1. Five types of wind turbines and four types of: PV modules, batteries, regulators, inverters and diesel generators were used respectively.

RESULTS AND DISCUSSION

The optimization of PV/wind/diesel generator/battery hybrid systems by minimizing the LCE and the CO_2
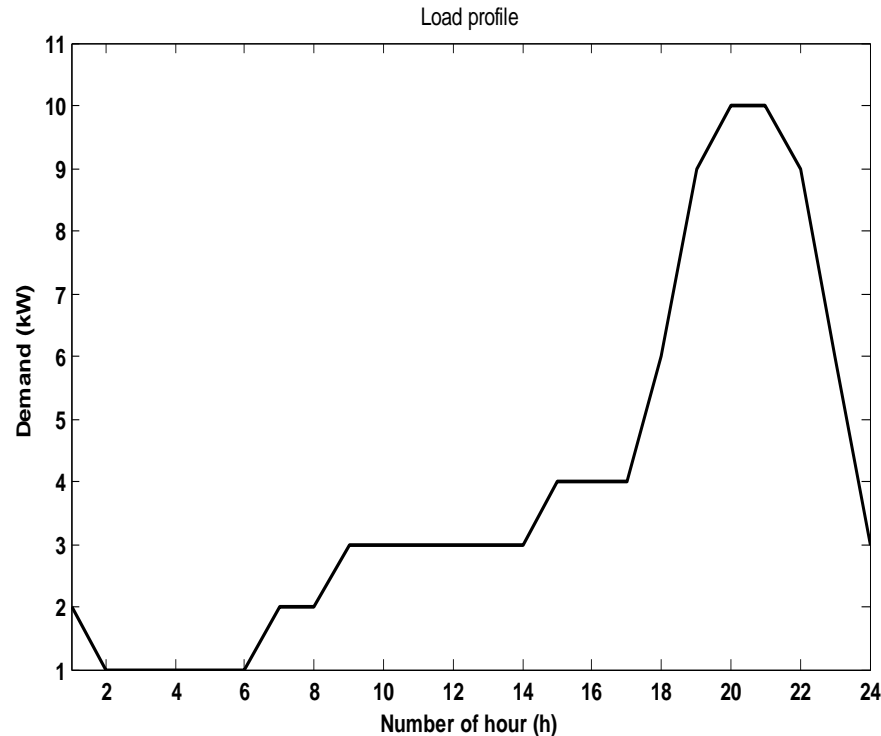
Load profile

Figure 4. load profile of the demand energy.

emission were carried out by using multi-objectives genetic algorithm approach. Obtained results have appeared as an optimal Pareto front. Every solution of the best Pareto front was formed by a combination of hybrid systems and control strategy, with a different LCE and the pollutant emission.

Figure 5 shows the optimal Pareto front between the LCE and the CO_2 emission. It was noted that the increasing of LCE implies the decreasing of the CO_2 emission. To illustrate the results given by Figure 5, five solutions (A, B, C, D and E) on different position of the Pareto front curve were indicated.

Table 2 depicts the size and the output energy of these five optimal solutions. It can be noted that the optimal type of the PV module, wind generator, battery bank, regulator, inverter and diesel generator was respectively the N°4, N°5, N°3, N°1, N°3, N°1 and N°3. It is, also, possible to note that the LCE decreases by 27 and 40% while passing from the solution A to solutions B and C respectively. That is because of the diminution of the components numbers of the system, specially the PV modules and the wind turbines in the systems. In the contrast, the diesel generator was more solicited, thus, the operation hours of diesel generator increases. For example the operations hours of the diesel generators pass from 6 h to 31 and to 119 h when the solution passes to B and C from A. So, the CO_2 emission increases by 89.40 kgCO_2/year and by 750.19

kgCO_2/year respectively when the solutions pass to B and to C from A. From Table 2, it can be seen as the PV modules and wind turbines decrease, the size of diesel generator increases. It can be also noted that the output energy from the wind turbine was lower (with fraction of 46% for the solution-A, 11% for the solution-B and 0% for the solution-C, D and E) compared to the output energy from PV generator. That can be explained by the higher potential of the solar and its variations which are more suitable to the variation of the load profile. The output energy from the diesel generators was lower for the solution A, B and C compared to solutions D and E. The highest fraction of the output energy observed for these three solutions was 16% observed for the solution C. The corresponding hours of operation was 119 h. However, the output energy from diesel generators was higher for the latest solutions (D and E) which are solutions without renewable energies (fraction of renewable energy was 0%). While, the amount of the CO_2 emitted was higher (4,870.37 and 10,839.55 kgCO_2/year respectively).

It can be noted from Table 2 that the battery bank was more solicited for the solution C (PV/diesel system). Figure 6 (solution-C) shows the distribution of the state of charge of this solution. It can be seen that the battery bank discharges up to 60 for 35% of the time. The lowest SOC was 43 observed for the solution-B, but this state of charge was observed for only 0.06% of time. The lowest average state of charge (SOC) was 75% observed for the

Table 1. Specifications of the components.

Specifications of the wind turbine						
Type of wind turbines	Cut-in wind speed Vci (m/s)	Rate wind speed Vr (m/s)	Cut-off wind speed Vco (m/s)	Rated power Pr (W)	Output voltage (V)	Cost (€)
1	2	9	12	500	48	3051
2	3.5	11	13	600	48	1995
3	3.5	12	12	1500	48	2995
4	2.5	14	25	5600	48	8870

Specifications of the PV module						
Type of of PV module	Rate voltage (V)	Nominal peak power k (W)	Current of short-circuit ¶(A)	Voltage of open circuit (V)	Fill factor	Cost (Euro)
1	12	75	4.70	21.50	0.74	590
2	12	80	5.31	21.30	0.71	540
3	12	100	6.46	20.00	0.77	559
4	12	150	8.40	21.60	0.74	900

Specifications of the batteries			
Type of batteries	Nominal capacity (Ah)	Nominal voltage (V)	Cost (Euro)
1	80	12	195
2	100	12	215
3	200	12	416
4	720	2	2059

Specifications of the regulators			
Type of the regulators	Nominal current (A)	Nominal voltage (V)	Cost (Euro)
1	30	48	230
2	40	48	250
3	45	48	289
4	60	48	295

Specifications of the inverters			
Type of the inverters	Nominal power (W)	Nominal voltage (V)	Cost (Euro)
1	3500	48	2799
2	2400	48	2165
3	4500	48	4185
4	5000	48	5350

Specifications of the diesel generators		
Type of diesel generator	Nominal output power	Cost (Euro)
1	3050	668
2	4000	862
3	4600	879
4	4860	895

solution-C and the highest (89%) was observed for the solution A. Figure 6 (solution-A), shows that the battery bank remain at the SOC 100% for 42% of time. So, the battery bank is less solicited. That allows the increasing of the lifetime of batteries, thus the diminution of the replacement cost of batteries.
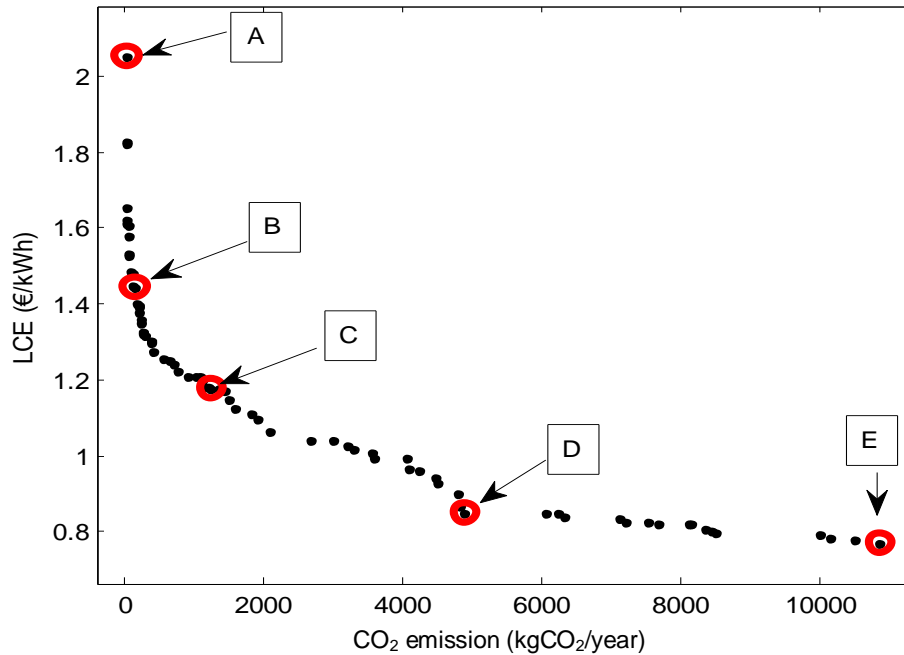
**Figure 5.** Optimal Pareto front of hybrid PV/wind/diesel/battery system

Table 2. Five solutions of the optimal pareto front.

Solution	Solution A	Solution B	Solution C	Solution D	Solution E
Number of PV modules	28	40	28	0	0
Number of Wind turbine	5	1	0	0	0
Number Batteries	60	60	64	48	24
Number of Regulators	2	3	2	0	0
Number of Inverters	5	5	5	5	5
Number Diesel generators	1	2	5	10	10
Type of Wind turbines	5	5	--	--	--
Type of PV modules	4	4	4	4	4
Type of Batteries	3	3	3	3	3
Type of Regulators	1	1	1	--	--
Type of Inverters	1	1	1	1	1
Type of diesel generators	3	3	2	3	3
Annual electrical energy delivered by PV generator (kWh/year)	26994.00	38563.00	26994.00	0.00	0.00
Annual electrical energy delivered by wind turbine (kWh/year)	23843.00	4768.60	0.00	0.00	0.00
Annual electrical energy delivered by diesel generator (kWh/year)	14.93	114.38	689.93	24102.70	25116.10
Annual operating hours of diesel (h)	6	31	119	4357	4589
Annual excess of energy (kWh/year)	28386.934	20980.38	5217.93	1636.70	2650.10
SCO_{min} (%)	56	43	55	61	60
Mean of SCO (%)	89	78	75	80	77
Annualized cost system of energy (€/kWh)	2.05	1.48	1.22	0.85	0.77
CO2 emission (kg CO2/year)	11.89	99.29	762.08	4870.37	10839.55

In order to highlight the hourly behavior of the obtained optimal configuration, the solution B (hybrid PV/wind/diesel/battery) has been used. A simulation was conducted on a period from 1st January to 19th February
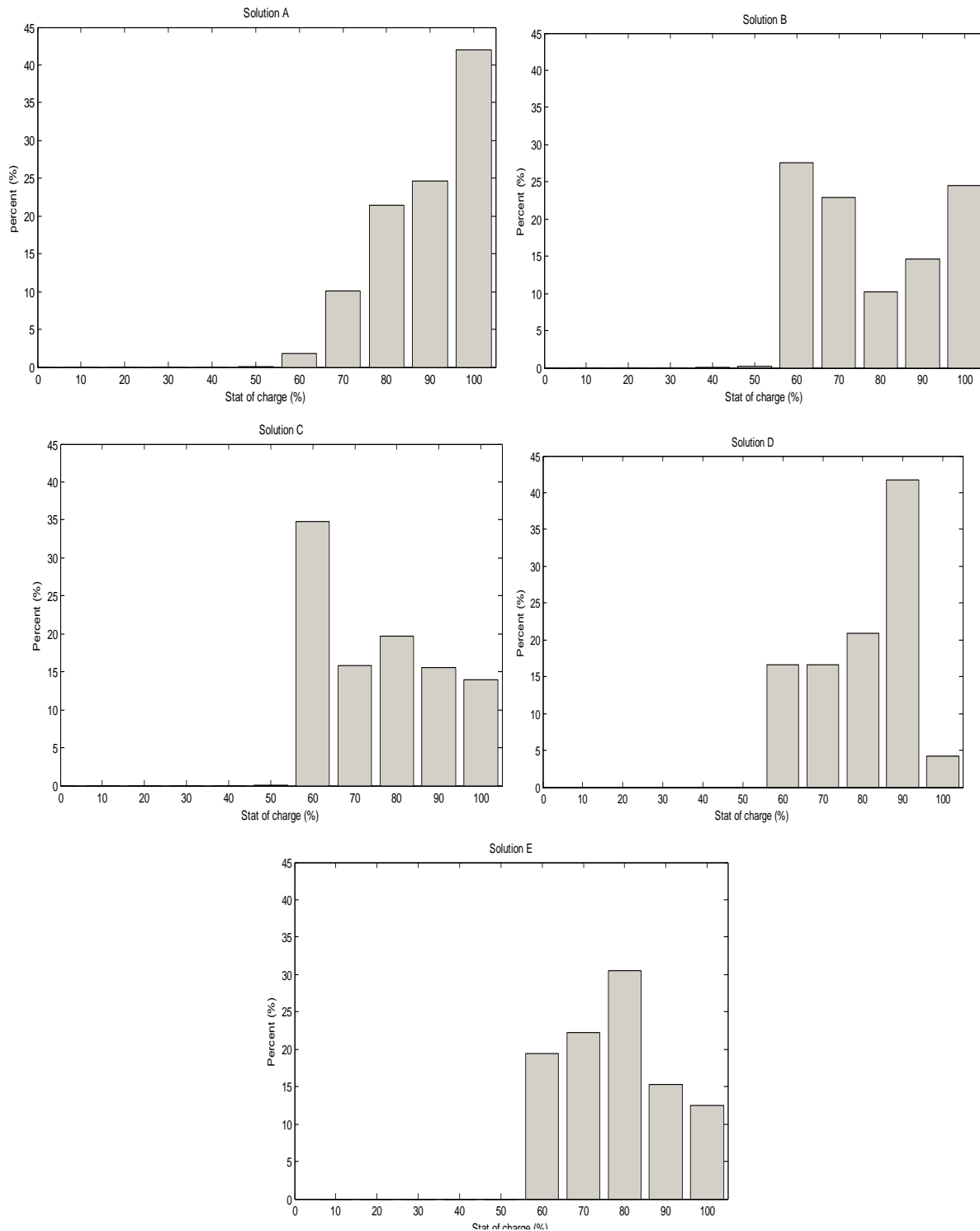
Figure 6. State of charge of the five solutions (A, B, C, D and E) of the Pareto front.

(12:00 hours) and is reported in Figure 7. Figure 7a, b, c and d show the output power from PV generator, wind turbine, the diesel generator and the output/input battery bank power. Figure 8 gives the state of charge of the battery bank for the indicated period.

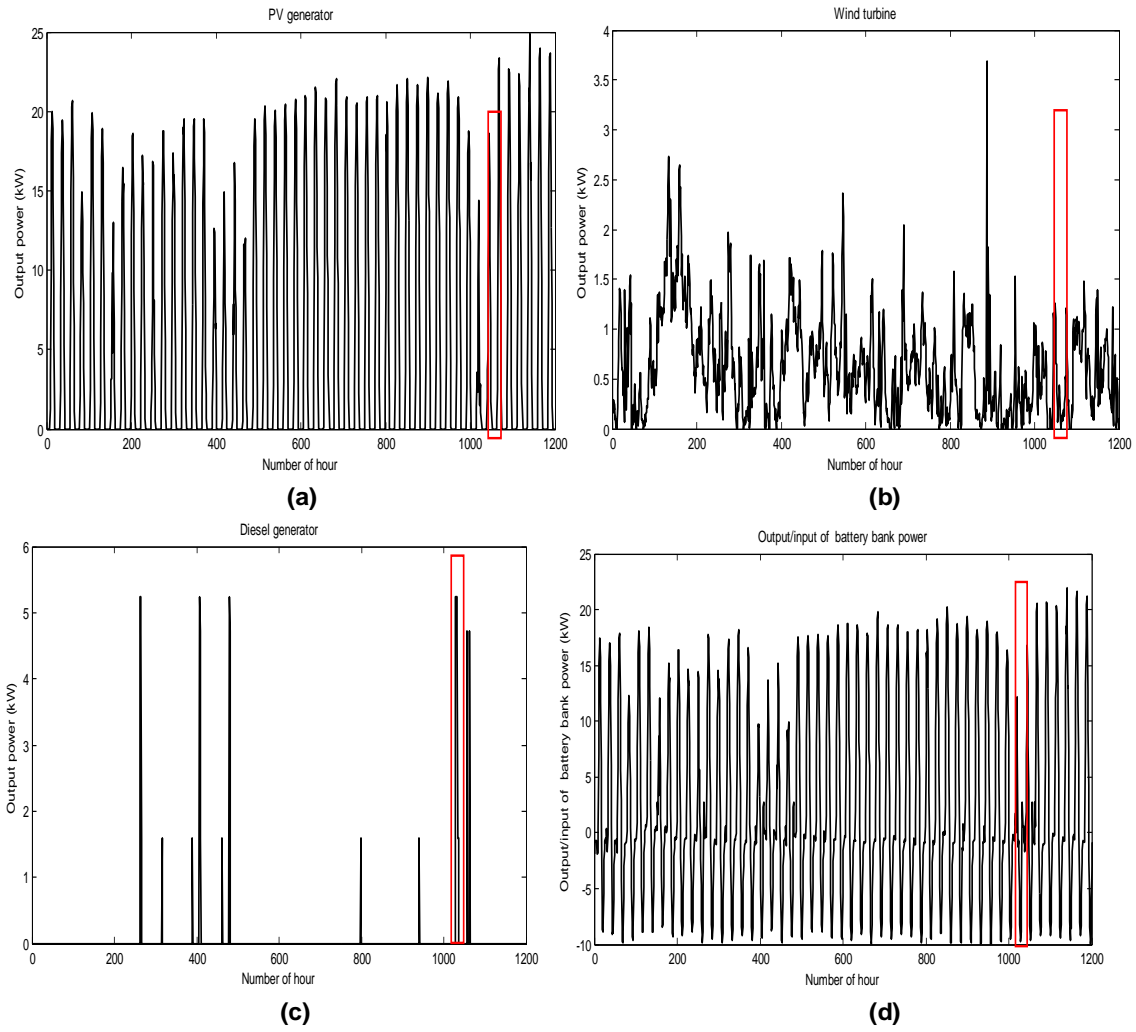According to the strategy denoted above and to the

Figure 7. Behavior of the PV generator, Wind turbine, Diesel generator and the battery bank (solution B).
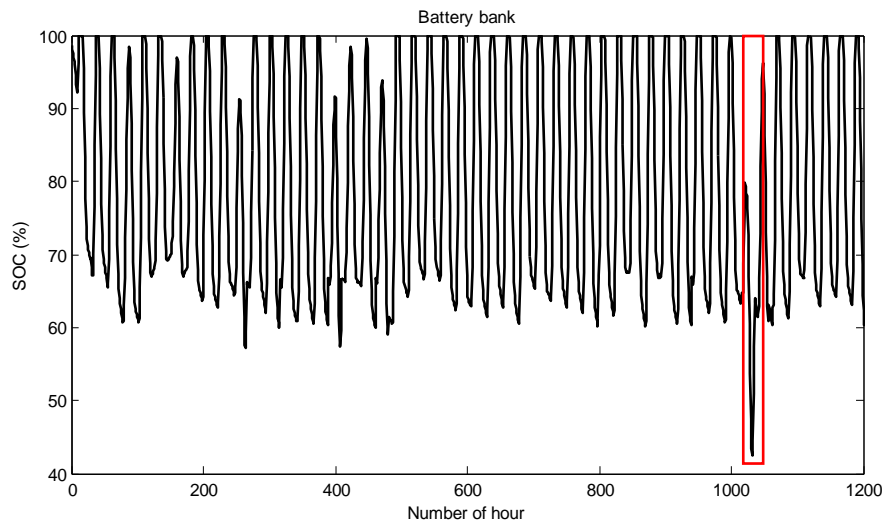

Figure 8. State of charge of the battery bank (solution B).

operation under the model constraints given by expression 7, it can be verified that, when the renewable sources power is greater than the power demand, the surplus power is stored in the battery bank, then $P_{bt} > 0$ (Figure 7a, b and d). When the renewable energy is smaller, the lack of energy is provided by the battery bank and or by the diesel generator (Figure 7c), then the $P_{bt} < 0$. Moreover, when the output energy from the PV generator and wind turbine is greater than the demand energy and the battery bank is fully charged then, the surplus of the energy produced can be used for the water pumping, water desalination, or to supply other demand of energy according to the needs of the village where the system is installed. From Figure 8, it can be seen that, the SOC remain between SOC_{max} (100%) and the SOC_{min} (40%). The minimum SOC achieved is 43% and observed for the 12th February at 23 h. In this hour of February day, it was noted 0 kW output energy from wind turbine and from PV generator. So the battery bank was deeply discharged and the diesel generator is operated to supply the load in the on hand and to charge the batteries in the other hand. The average of the SOC during this period of operations (1st January to 19th February) was 75% and the hour number of diesel generator time operation was 19 h.

Conclusion

The methodology for optimal sizing of multi-objective hybrid PV/wind/diesel/battery bank systems minimizing the LCE and the CO_2 emission by using a Genetic Algorithm approach was developed in this paper. The obtained results were depicted on the optimal Pareto front. From the results, we can outline the following points:

(i) The increasing of the LCE implies the decreasing of the CO_2 emission.
(ii) The LCE decreases by 27 and 40 % while passing from the solution A to the solutions B and C. In the contrast the CO_2 emission increases by 89.40 $kgCO_2$/year and 750.19 $kgCO_2$/year respectively when the solutions pass to B and C from A.
(iii) The PV generator was more solicited than the wind turbine generator for the hybrid PV/wind/diesel/batteries in the site of Potou. For the solutions, the highest fraction of the wind turbine was 46% observed for the solution A.
(iv) The only PV/battery or Wind/ battery were not an optimal configuration for this application on the site of Potou with the use of the load profile and the indicated specifications of the devices. It would be interested to perform modeling, incorporating the objectives of availability and reliability constraints of components to achieve a more accurate assessment of the cost of ownership system.

Conflict of Interest

The authors have not declared any conflict of interest.

REFERENCES

Ahmad R, Kazem M, Hossein K (2010). Modeling of a Hybrid Power System for Economic Analysis and Environmental Impact in HOMER. IEEE. 978-1-4244-6760-0.

Ahmed MAH, Priscilla NJ and Mohd S (2011). Optimal configuration assessment of renewable energy in Malaysia. Renewable Energy. 36:881-888.

Ajay KB, Gupta RA, Rajesh K (2011). Optimization of Hybrid PV/wind Energy System using Meta Particle Swarm Optimization (MPSO). IEEE. 978-1-4244-7882-8.

Alam HM, Manfred D (2010). Hybrid systems for decentralized power generation in Bangladesh. Energy for Sustainable Development. 14:48–55.

Anvari Moghaddam A, Seifi A, Niknam T, Alizadeh Pahlavani MR (2011). Multiobjective operation management of a renewable MG (micro-grid) with backup micro-turbine/fuel cell/battery hybrid power source. Energy 36:6490-6507.

Ayong H, Rudi K, Managam R, Yohannes MS, Junaidi M (2013). Techno-economic analysis of photovoltaic/wind hybrid system for onchore/ remote area in Indonesia. Energy 59:652-657.

Azizipanah-Abarghooee R, Niknam T, Roosta A, Malekpour AR, Zare M (2012). Probabilistic multiobjective wind-thermal economic emission dispatch based on point estimated method. Energy 37:322-335.

Bahtiyar D (2012). Determination of the optimum hybrid renewable power generating systems for Kavakli campus of Kirklareli University, Turkey. Renewable Sustainable Energy Rev. 16:6183–6190.

Bekele G, Palm G (2010). Feasibility study for a standalone solar–wind-based hybrid energy system for application in Ethiopia. Appl. Energy. 87(2):487–495.

Belfkira R, Zhang L, Barakat G (2011). Optimal sizing study of hybrid wind/PV/diesel power generation unit. Solar Energy 85:100-110.

Belgin ET, Ali YT (2011). Economic analysis of standalone and grid connected hybrid energy systems. Renewable Energy 36:1931-1943.

Chong L, Xinfeng G, Yuan Z, Chang X, Yan R, Chenguang S, Chunxia Y (2013). Techno-economic feasibility study of autonomus hybrid wind-PV-battery power system for a household in Urumqi, China. Energy 55:263-272.

Coello CA, Veldhuizen DAV, Lamont GB (2002). Evolutionary algorithms for solving multi-objective problems. New York: Kluwer Academic/Plenum Publishers.

Colle S, Abreu SL, Ruther R (2004). Economic evaluation and optimisation of hybrid diesel/photovoltaic systems integrated to electricity grid. Solar Energy 76:295–299.

Dalton GJ, Lockington DA and Baldock TE (2009). Feasibility analysis of renewable energy supply options for a grid-connected large hotel. Renewable Energy 34:955–964.

Diaf S, Notton G, Belhamel M, Haddadi M, Louche A (2008). Design and techno-economical optimization for hybrid PV/wind system under various meteorological conditions. Appl. Energy 85(10):968–987.

Duffo-Lopes R, Bernal- Agustin JL (2008). Multio-bjective design of wind-diesel-hydrogen-battery systems. Renewable Energy 33:2559-2572.

Duffo-Lopes R, Bernal- Agustin JL (2005). Design and control strategies of PV-Diesel systems using genetic algorithm. Solar Energy 79:33-46.

Eyad SH (2009). Techno-economic analysis of autonomous hybrid photovoltaic-diesel-battery system. Energy for Sustainable Development. 13:143–150.

Ekren O, Ekren BY (2010). Size optimization of a PV/wind hybrid energy conversion system with battery storage using simulated annealing. Appl. Energy 87(2):592–598.

Ekren O, Ekren BY (2008). Size optimization of a PV/wind hybrid energy conversion system with battery storage using response surface methodology. Appl. Energy 85:1086-1101.

Fleck B, Huot M (2009). Comparative life-cycle assessment of a small wind turbine for residential off-grid use. Renewable Energy 34:2688-2696.

Guasch D, Silvestre S (2003). Dynamic battery model for photovoltaic applications. Prog Photovoltaics: Res. Appl. 11:193–206.

Gupta A, Saini RP, Sharma MP (2011). Modelling of hybrid energy system d Part I: Problem formulation and model development. Renewable Energy 36:459-465.

Hongxing Y, Wei Z, Chengshi L (2009). Optimale design and techno-economic analysis of a hybrid solar-wind power generation system. Appl. Energy 86:163-169.

Ismail MS, Moghavvemi M, Mahlia TMI (2014). Genetic algorithm based optimization on modeling and design of hybrid renewable energy systems. Energy Convers.Manage. 85:120–130.

Ismail MS, Moghavvemi M, Mahlia TMI (2013). Techno-economic analysis of an optimized photovoltaic and diesel generator hybrid power system for remote houses in a tropical climate. Energy Conversion and Management. 69:163–173.

Kanase-Patil AB, Saini RP, Sharma MP (2011). Sizing of integrated renewable energy system based on load profilesand reliability index for the state of Uttarakhand in India. Renewable Energy 36:2809-2821.

Kalantar M, Mousavi GSM (2010). Dynamic behavior of a stand-alone hybrid power generation system of wind turbine, micro turbine, solar array and battery storage. Appl. Energy 87(10):3051–3064.

Kellogg WD, Nehrir NH, Venkataramanan G, Gerez V (1998). Generation unite sinzing and cost analysis for stand-alone wind, photovoltaïque and hybrid wind/PV systems. IEEE transaction on Energy Convers. 13(1):70-75.

Koutroulis E, Kolokotsa D, Potirakis A, Kalaitzakis K (2006). Methodology for optimal sizing of stand-alone photovoltaic/wind generator systems using genetic algorithms. Solar Energy 80:1072-1088.

Kyoung-Jun L, Dongsul S, Dong-Wook Y, Han-Kyu C, Hee-Je Kim (2013). Hybrid photovoltaic/diesel greenship operating in standalone and grid-connected mode – Expeimental Investigation. Energy. 49:475-483.

Leyland G (2002). Multi-objective optimization applied to industrial energy problems.188p. Thèse EPFL, n°: 2572 Lausanne.

Mei SN, Chee WT (2012). Assessment of economic viability for PV/wind/diesel hybrid energy system in southern Peninsular Malaysia. Renewable Sustainable Energy Rev. 16:634–647.

Mir-Akbar H, Hugh C, Christopher S (2011). A feasibility study of hybrid wind power systems for remote communities. Energy Policy 39:877–886.

Mohammad RN, Ali AV, Rasoul AA, Mahshid J (2014). Enhanced gravitational search algorithm for multi-objective distribution feeder reconfiguration considering reliability, loss and operational cost. IET Generation, Transmission & Distribution. 1:55–69.

Mohammad RN, Rasoul AA, Behrouz ZMS, Kayvan G (2013). A novel approach to multi-objective optimal power flow by a new hybrid optimization algorithm considering generator constraints and multi-fuel type. Energy 49:119-136.

Molyneaux A (2002). A practical evolutionary method for the multi-objective optimization of complex integrated energy systems including vehicul drive-trains. Thèses EPFL, n°: 2636, Lausanne. 194 pp.

Mukhtaruddin RNSR, Rahman HA, Hassan MY, Jamian JJ (2015). Optimal hybrid renewable energy design in autonomous system usingIterative-Pareto-Fuzzy technique. Electrical Power Energy Systems. 64:242–249.

Muyiwa SA, Samuel SP and Olanrewaju MO (2014). Assessment of decentralized hybrid PV solar-diesel power system for applications in Northern part of Nigeria. Energy Sustainable Dev. 19:72–82.

Ould Bilal B, Ndiaye PA, Kebe CMF, Sambou V, Ndongo M (2012a). Methodology to Size an Optimal Standalone Hybrid Solar-Wind-Battery System using Genetic Algorithm. Int. J. Phys. Sci. 7(18):2647-2655.

Ould Bilal B, Sambou V, Kebe CMF, Ndiaye PA and Ndongo M (2012b). Methodology to Size an Optimal Stand-Alone PV/wind/diesel/battery System Minimizing the Levelized cost of Energy and the CO2 Emissions. Energy Procedia 14:1636-1647.

Ould Bilal B, Sambou V, Ndiaye PA, Kebe CMF, Ndongo M (2010). Optimal design of a hybrid Solar-Wind-Battery System using the minimization of the annualized cost system and the minimization of the loss of power supply probability (LPSP). Renewable Energy 35:2388-2390.

Patrick MM, Sennoga T and Ines SM (2014). Analysis of the cost of reliabkle electricity: A new method for analyzing grid connected solar, diesel and hybrid distributed electricity systems considering an unreliable electric grid with exemples in Uganda. Energy 66:523-534.

Prabodh B, Vaishalee D (2012). hybrid renewable energy systems for power generation in stand-alone application: A review. Renewable Sustainable Energy Rev. 16:2926-2939.

Rohit S, Subhes CB (2014). Off-grid electricity generation with renewable energy technologies in India: An application of HOMER. Renewable Energ. 62:388-398.

Saheb-Koussa D, Haddadi M, Belhamel M (2009). Economic and technical study of a hybrid system (wind–photovoltaic–diesel) for rural electrification in Algeria. Appl. Energy 86:1024-1030.

Sambou V (2008). Transferts thermiques instationnaires: vres une optimisation de parois de bâtiments. Thèse, PHASE, Université Paul Sabatier. 195 pp.

Sanjoy K, Himangshu RG (2009). A wind–PV-battery hybrid power system at Sitakunda in Bangladesh. Energy Policy. 37:3659–3664.

Senjyu T, Hayashi D, Yona A, Urasaki N and Funabashi T (2007). Optimal configuration of power generating systems in island with renewable energy. Renewable Energy 32:1917-1933.

Shen WX (2009). Optimally sizing of solar array and batteriy in a standalone photovoltaic system in Malaysia. Renewable Energy 34:348-352.

Sonntag RE, Borgnakke C, Wylen GJV (2002). Fundamentals of thermodynamics, 6th ed. New York: Wiley.

Suresh-Kumar U, Manoharan PS (2014). Economic analysis of hybrid power systems (PV/diesel) in different climatic zones of Tamil Nadu. Energy Convers. Manage. 80:469–476.

Yang HX. Burnett L, Weather JL (2003). Data and probability analysis of hybrid photovoltaic–wind power generation systems in Hong Kong. Renewable Energy 28:1813–1824.

Yang HX, Lu L (2004). Study on typical meteorological years and their effect on building energy and renewable energy simulations. ASHRAE Transactions 110(2):424–431.

Yang HX, Lu L, Zhou WA (2007). Novel optimization sizing model for hybrid solar–wind power generation system. Solar Energy 81(1):76–84.

Yang HX, Zhou W, Lu L, Fang Z (2008). Optimal sizing method for stand-alone hybrid solar-wind system with LPSP technology by using genetic algorithm. Solar Energy 82:354-367.

Zeinab AME, Muhammad FMZ, Kamaruzzaman S, Abass AA (2012). Design and performance of photovoltaic power system as a renewable energy source for residential in Khartoum. Int. J. Phys. Sci. 7(25):4036-4042.

Zhou W, Lou C, Li Z, Lu L, Yang H (2010). Current status of research on optimum sizing of stand-alone hybrid solar–wind power generation systems. Appl. Energy 87:380–389.

International Journal of Physical Sciences

Related Journals Published by Academic Journals

- African Journal of Pure and Applied Chemistry
- Journal of Internet and Information Systems
- Journal of Geology and Mining Research
- Journal of Oceanography and Marine Science
- Journal of Environmental Chemistry and Ecotoxicology
- Journal of Petroleum Technology and Alternative Fuels

academicJournals